Glen Oumellal

Prediction of Quiescent Periods in Linear Wave Theory with the Prony Method

Master's thesis in Civil and Environmental Engineering
Supervisor: Michael Muskulus
June 2023

NTNU

Norwegian University of
Science and Technology

Glen Oumellal

Prediction of Quiescent Periods in Linear Wave Theory with the Prony Method

Master's thesis in Civil and Environmental Engineering
Supervisor: Michael Muskulus
June 2023

Norwegian University of Science and Technology
Faculty of Engineering
Department of Civil and Environmental Engineering

Abstract

Some marine operations such as helicopter landing on a deck require low motions of the vessel, called *Quiescent Periods* (QPs). QP prediction methods are used to determine the short-term future calm opportunities, to safely perform the operation. A new tool for signal filtering has recently gained attention: the Prony method. It consists in fitting a sum of exponential components to the signal. In this context, this thesis applies the Prony tool to QP prediction and evaluates the prediction quality.

Based on a JONSWAP wave spectrum, the waves and the motions are modelled within the linear theory. This thesis presents the occurrence statistics of QPs, both in the waves and the modelled vessel motions. These statistics could constitute a tool for marine operations planning. This work then describes the Prony method, with an implementation in MATLAB of a least squares Prony algorithm applied to wave prediction. The prediction quality is discussed with the parameters of the analysis. A preliminary filtering of the signal was found to significantly increase the prediction quality. The Prony method obtains reliable predictions of 20 seconds for the waves, and reaches 30 seconds for the vessel motions.

Sammendrag

Marine operasjoner slik som helikopterlanding på et dekk offshore krever små bevegelser i fartøyet, kalt stille perioder (*Quiescent Periods* på engelsk). En prediksjonsmetode for stille perioder kan brukes til å bestemme fremtidige rolige tidsrom på kort sikt, for å utføre operasjonen på en sikker måte. Et nytt verktøy for signalfiltrering har nylig fått oppmerksomhet: Prony metoden. Den består av å tilpasse en sum av eksponentielle komponenter til signalet. Denne oppgaven bruker Prony metoden til å predikere stille perioder og evaluerer prediksjonskvaliteten.

Basert på et JONSWAP bølgespektrum er bølgene og bevegelsene modellert med lineær bølge teori. Denne oppgaven presenterer statistikken knyttet til stille perioder, både for bølgene og de modellerte fartøybevegelsene. Dette utgjør et verktøy for planlegging av marine operasjoner for en gitt sjøgang. Deretter beskrives Prony metoden, med en minste kvadraters Prony algoritme brukt til bølgeprediksjon, i MATLAB. Prediksjonskvaliteten med hensyn til parameterne i analysen er diskutert. Kvaliteten økte betydelig ved å etablere og inkludere filtrering av signalet. Prony metoden oppnådde pålitelige prediksjon på 20 sekunder for bølgene, og hele 30 sekunder for fartøyets bevegelser.

Acknowledgements

First and foremost, I am extremely thankful to my supervisor, Michael Muskulus, for his guidance throughout this journey. His invaluable feedback and expertise made this work possible. His benevolence and enthusiasm throughout this semester made it a pleasure to work under his supervision.

I would also like to show my gratitude to every member of the research group: Adriana Correia da Silva, David Oyegbile, Jing Dong, Ane Bjerkebæk and Kutay Yilmazlar. Their comments and experiences helped me make this thesis a success. In particular, I would like to thank Ane for her help with the translation of the abstract.

Special thanks to Helen Tobback for her precious feedback during the writing process.

Finally, I would like to extend my gratitude to my friends, my family and my girlfriend for their support during this process. This accomplishment would not have been possible without them. Thank you.

Table of Contents

1 List of Figures

2 List of Abbreviations

AE	Absolute Error
ARMA	Auto-Regressive Moving Average
DSWP	Deterministic Sea Wave Prediction
JONSWAP	Joint North Sea Wave Observation Project
LS	Least Squares
MaAE	Maximum Absolute Error
QP	Quiescent Period
RAO	Response Amplitude Operator
RMSE	Root Mean Square Error
TLS	Total Least Squares

1 Introduction

Marine operations are often limited by sea conditions. In large seas, the decision to perform maneuvers such as helicopter landing on a ship, cargo hoisting from a vessel to an offshore platform or maintainance activities can either lead to excessive risks or the cancelation of the task. Due to the recent improvements in computational resources and techniques, a new branch of oceanography has emerged: Deterministic Sea Wave Prediction (DSWP). It aims at predicting short-term incoming waves, and has to be distinguished from the statistical description of waves that has been used for decades.

In most sea conditions, groups of large waves often alternate with calmer periods. Such interval is termed *Quiescent Period* (QP), from the Latin root *quiescere* (rest, quiet). The new DSWP methods are now able to predict the incoming waves and the occurrence of calm periods a few seconds in advance, which can be of effective help for the safety and the success of marine operations.

QPs can refer to two phenomena: calm periods in the sea surface elevation, in other words waves, or small motions of a vessel at sea. In the first case, a calm period is a group of waves with small amplitudes, where the critical amplitude is called threshold, as shown in Figure 1. In the second case, QPs refer to time intervals when the motions of interest are below a defined amplitude, either one motion at a time or all motions of interest which can be more restrictive.
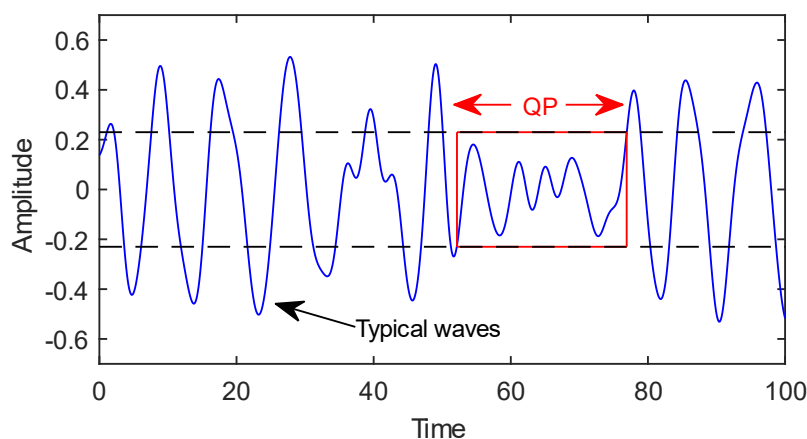
Figure 1: Example of a quiescent period in a signal

The minimum time length of a QP depends on the performed task, but is usually between ten seconds and a few minutes. For example, a helicopter landing on a ship requires a time window of twenty to thirty seconds, while firing operations on a military vessel can take up to one minute.

Two main methodologies exist for QP prediction: *looking backwards* and *looking forward*. These methods are summarized in Giron-Sierra & Esteban (2010), and Sherman (2007) provides an extensive bibliography and an evaluation of the different QP prediction methods.

The idea of the methods that look back in the past is to record the recent ship motions, and fit it to a model via a filter to predict the future motions. Different signal filters have been used since the late 1960s, first claiming 6 seconds of prediction horizon

(Dalzell, 1965; Kaplan, 1969). In the 80s, an ARMA model (Auto-Regressive Moving Average) was introduced (Yumori, 1981), and then improved to obtain up to 10 seconds of prediction with respect to roll and 15 seconds for pitch and heave. Most of these methods try to fit a given model to the wave envelope and proceed to a signal continuation. They are real-time methods and are computed in less than a second.

The *looking forward* methods have appeared more recently, with the spread of radar imaging. The three main tasks of this methodology are: measuring incident waves with enough distance; applying a propagation model to compute wave deformation as it moves towards the ship; computing the ship motions with a model of the ship dynamics. The new radar imaging methods are now able to measure incident waves up to three nautical miles (5.5 km) (Nieto Borge et al., 2004). New propagation models based on wavelet analysis have been able to predict QPs up to two minutes in advance (Dong et al., 2008). In contrast with the Fourier analysis, wavelet models can analyse the frequency contents of a signal in the time domain. Thus, it can be used for non-stationary signals, while the Fourier transform is adapted to stationary signals. However, these methods require heavy computations.

The aim of this study is to implement a new method for QP prediction that enters the first category of these methodologies. Based on the Prony analysis, it consists in fitting a sum of damped sinusoids to the waves. First introduced by Gaspard de Prony who studied expansion characteristics of gases (Prony, 1795), this method has recently gained attention due to advances in computer systems. It has now applications in various engineering sectors such as electric power quality analysis, fluid dynamics or biomedical signal filtering (Duclos et al., 2001; Fernández Rodríguez et al., 2018; Zygarlicki & Mroczka, 2012).

This thesis first focuses on the modelling of irregular waves and vessel motions in linear theory and the use of sea state spectra, as well as statistical properties of quiescent periods. This work then describes the theory behind Prony analysis, and implements an algorithm based on the least squares Prony method in MATLAB. In the last section, the Prony method is used for wave prediction, and the influence of the main parameters on the prediction quality is presented.

2 Irregular waves and ship motion modelling

This thesis describes the implementation of the Prony analysis in a signal. It can be used directly on the wave surface elevation signal, but the real applications of QP prediction methods are often based on vessel motions. A transfer function is applied to the incident waves signal, resulting in the motions of interest for a certain ship such as heave, pitch and roll.

The choice was made to create times series as modelled surface elevation signals, and not to use real measurements. The reader must keep this in mind regarding all results and conclusions.

2.1 Irregular waves model with linear theory

The time series are generated with the use of an oceanographic spectrum, the JONSWAP (Joint North Sea Wave Observation Project) spectrum. This spectrum is commonly used for engineering applications when analysing irregular waves. It provides information on wave energy distribution for idealized conditions, namely a sea state after a constant wind has been blowing for some time. A real spectrum would be more sophisticated, with several peaks referring to different swells, and would require an additional information on the direction of the waves. For simplicity, a unidirectional model is considered.

This spectrum is a parameterized function defining the wave energy distribution with respect to the wave frequency. A formulation depending on the significant wave height H_s and the peak period T_p (or peak angular frequency $\omega_p = 2\pi/T_p$) was proposed by Goda (1988):

$$S(\omega) = \beta H_s^2 \frac{\omega_p^4}{\omega^5} \exp\left[-\frac{5}{4}\left(\frac{\omega}{\omega_p}\right)^{-4}\right] \cdot \gamma^r, \tag{1}$$

in which

$$\gamma \in [1,7],$$

$$r = \exp\left[-\frac{1}{2\sigma}\left(\frac{\omega}{\omega_p} - 1\right)^2\right],$$

$$\sigma = \begin{cases} 0.07, \text{if } \omega \leq \omega_p, \\ 0.09, \text{if } \omega > \omega_p, \end{cases}$$

$$\beta = \frac{0.0624 \cdot (1.094 - 0.01915 \cdot \ln(\gamma))}{0.23 + 0.0336 \cdot \gamma - 0.185/(1.9 + \gamma)}.$$

The constant γ is called the peak-enhancement factor. Although it can vary between the different regions of the world, its mean value $\gamma = 3.3$ is usually considered, as in this study. Figure 2 shows examples of JONSWAP spectra for multiple values of H_s and T_p, and $\gamma = 3.3$.
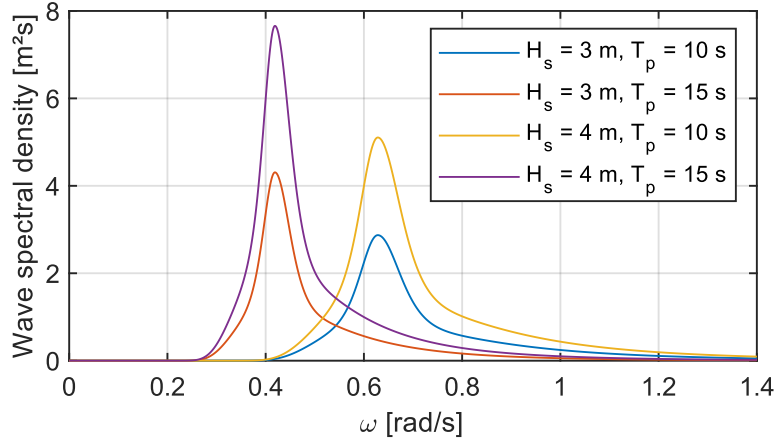
Figure 2: The JONSWAP spectrum shape

This spectrum forms the basis for the creation of the signal. In this thesis, we consider linear waves in infinite deep water: the sea state is a sum of n sinusoids with angular frequencies ω_j regularly distributed. The amplitudes are directly computed from the spectrum: a high spectral density leads to a high amplitude for the given component. The surface elevation at a given point in space is computed by the random phase model:

$$X(t) = \sum_{j=1}^{n} A_j \cdot \cos\left(\omega_j t + \varphi_j\right), \tag{2}$$

in which for each component indexed by j:

$$A_j = \sqrt{2S(\omega_j)\Delta\omega},$$

$$\varphi_j \in [0,2\pi[.$$

The phases are randomly generated, making the signal similar to irregular waves. $\Delta\omega$ refers to the interval between two successive angular frequencies. This model has a widespread use in marine engineering, and is a very simple way to create simulations of waves in an irregular sea state. In this thesis, these generated signals are used for wave prediction.

2.2 Vessel motions model

As most marine operations are performed on a ship, the prediction methods are often based on vessel motions. The modelling of ship dynamics is extremely complex, but a simple approach consists in using simple uncoupled transfer functions $H(\omega)$ for each motion. A transfer function is a complex function that describes the system's output, here the vessel motions, based on the input, the waves, for each component of frequency ω. It contains two pieces of information: the output's amplitude and phase. The amplitude of $H(\omega)$ describes how a frequency component is amplified or reduced in the output, while the phase results in the time shift between the input and the output.

When modelling ship motions, we often only consider heave, pitch and roll. The response spectra are then given by the following expression:

$$R(\omega) = |H(\omega)|^2 \cdot S(\omega). \tag{3}$$

14
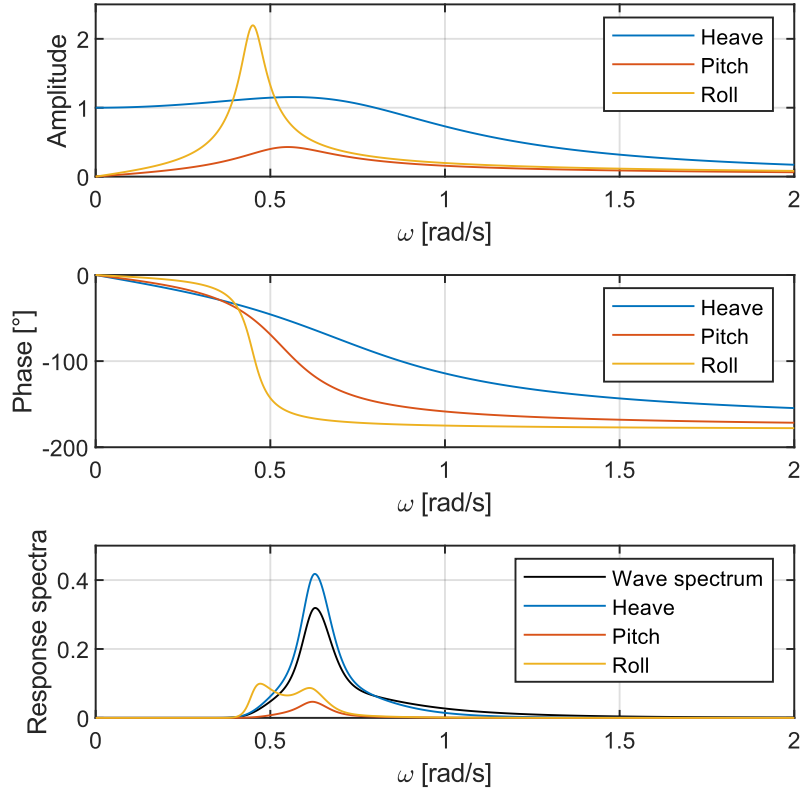
Figure 3: Transfer functions and response spectra for the vessel motions

Figure 3 shows realistic transfer functions for heave, pitch and roll and the associated response spectra for a ship. The wave spectrum that was used is a JONSWAP spectrum with standard values of $H_s = 1\,\text{m}$, $T_p = 10\,\text{s}$ and $\gamma = 3.3$. The units of the amplitude $|H(\omega)|$ are $[\text{m/m}]$ for heave and $[\text{rad/m}]$ for pitch and roll. For the response spectra, $R(\omega)$ is given in $[\text{m}^2\text{s}]$ for heave and $[\text{rad}^2\text{s}]$ for pitch and roll. No ship speed is considered, and the encounter frequency, which is the frequency seen from the ship, is the same as the wave frequency. Implementing a non-zero speed would result in a shift in frequencies of the motion spectra, affecting the response. For simplicity the motionless case only is studied, but the case of non-zero speed will be discussed later.

These RAOs (Response Amplitude Operators) will be used for the rest of the thesis to compute the motions of a ship. From the response spectra, the motions are reconstructed the following way:

$$M(t) = \sum_{j=1}^{n} \sqrt{2R(\omega_j)d\omega} \cdot \cos\left(\omega_j t + \varphi_j + \text{phase}\left(H(\omega_j)\right)\right). \qquad (4)$$

Figure 4 presents a time series realization of the waves and the motions of interest. The QPs are framed in red. The QPs that are in common between the three motions are highlighted with a black dotted line.
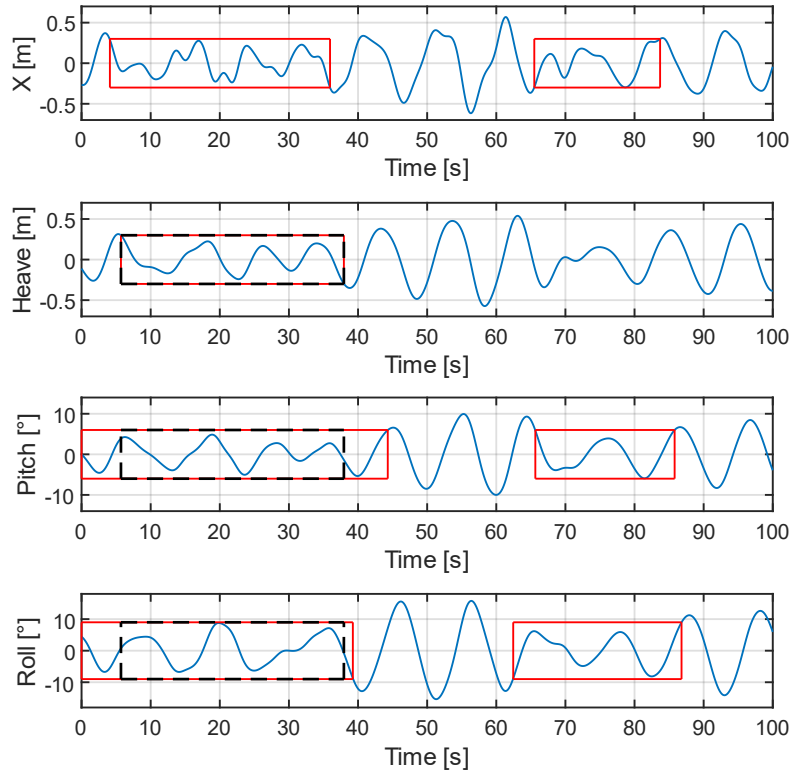
Figure 4: Time series realization of irregular waves and vessel motions, with threshold heights of $0.3\,\mathrm{m}$ for waves and heave, $6°$ and $9°$ for pitch and roll respectively, and a minimum QP length of $15\,\mathrm{s}$

A time interval is detected as a QP if the maximum of the absolute value of the signal stays below a given threshold height, called A_{max}, for a minimum time denoted T_{min}. For example, Figure 4 was created with threshold heights of $0.3\,\mathrm{m}$ for waves and heave, $6°$ and $9°$ for pitch and roll respectively. The minimum length of a QP was set to $15\,\mathrm{s}$.

3 Statistics of quiescent periods

When an operation needs to be performed, the stakeholders involved first examine the conditions, the chances of success, and the possibility to find a time window that is long enough to execute the mission. It can be a precious advantage to study quiescent periods statistics for given sea state conditions: the decision-makers could decide if the chance to find proper quiescent periods is high enough for the operation to be performed.

In this thesis, we focus on the quality of QP prediction for the presented waves model. A critical parameter is the number of components in the waves signal, n. The properties of the signal vary with this number, in the same way QP prediction does. Thus, highlighting QP statistics for different numbers of wave components is relevant here. Three numbers of components will be used in this part: $n_1 = 20$, $n_2 = 100$ and $n_3 = 1,000$.

All statistics are computed numerically in MATLAB, by generating m signals of length T_{max} and detecting the quiescent periods. T_{max} is usually set to $100T_p$. The minimum QP length (the minimum time for a period to be detected as quiescent) is denoted T_{min}, and is usually higher than $2T_p$, as most marine operations require at least 20 seconds to be performed.

3.1 Length and proportion of quiescent periods in waves

The first quantity of interest for the decision-makers is the time length of quiescent periods for a given threshold height.

Al-Ani et al. (2019) give some results on such statistical properties, based on probability distribution models for QPs. This paper gives the probability of quiescent runs of a certain number of waves, for different thresholds, and the mean duration of these QPs. In the present work, the QPs intervals are continuous and we deal with time length instead of runs of waves. Similarities with regards to QP distributions were noted, as presented later.

The JONSWAP spectrum might play an important role in the QP statistics. Figure 5 shows the mean length of QPs with respect to the threshold height. It was computed from three spectra with different peak periods but the same significant height, for $n_2 = 100$ components. The minimum length of a QP is set to $T_{min} = 2T_p$, which is dependent on the spectrum. It also displays the scaled mean length of these QPs, for which the mean length is divided by the peak period.
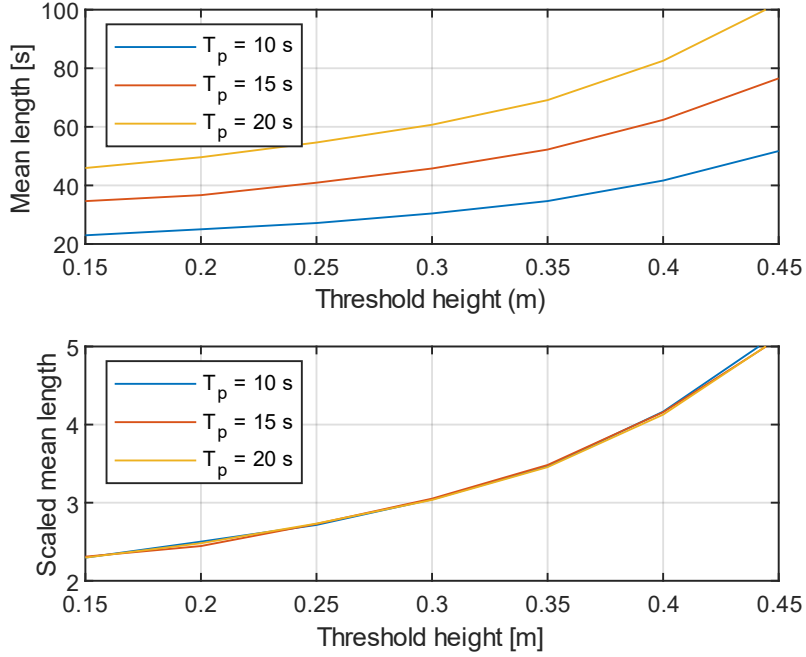
Figure 5: Mean length and scaled mean length of QPs, for three JONSWAP spectra with different peak periods

The scaled mean length is similar for the three spectra: this underlines the independence of statistical properties from the parameter T_p. Indeed, a multiplication by a factor k of ω_p leads to a multiplication of all frequencies by the same factor. We can show from equations (1) and (2) that the new signal is simply stretched in the time domain by this factor. Likewise, the statistics are independent from the significant wave height H_s if we scale the threshold. Consequently, all properties and predictions are independent from H_s and T_p after the scaling step. This is proved in Appendix 1.

Thus, all computations can be performed with the same JONSWAP parameters. For simplicity, we choose $H_s = 1\,\text{m}$ and $T_p = 10\,s$. In this thesis, QP lengths and threshold heights are given unscaled, for a better physical understanding of the properties. This result also proves that quiescent periods will be longer for sea states with higher peak periods: when the swell is dominant, a higher peak period implies longer quiescent periods. Regarding the encounter frequency of a moving ship, a shift in the wave spectrum would have a similar effect and either lead to shorter wave periods in the case of sailing towards the waves or longer waves when sailing in the same direction, and so longer or shorter QPs respectively. One would then say that it is better to sail in the same direction as the waves. However, in reality ships often sail towards the waves to increase stability at high seas, leading to a shift in high frequencies. This could be explained by the fact that a vessel acts as a low-pass filter. Thus, sailing in the waves instead of sailing in the same direction reduces the response of the ship and increases stability.

For the standard values of the JONSWAP spectrum, Figure 6 shows the mean length of QPs for n_1, n_2 and n_3, for a minimum QP time of $T_{min} = 2T_p = 20\,s$. The average proportion of QPs that compose the signal is computed, in other words the probability to be in a QP at a random time.
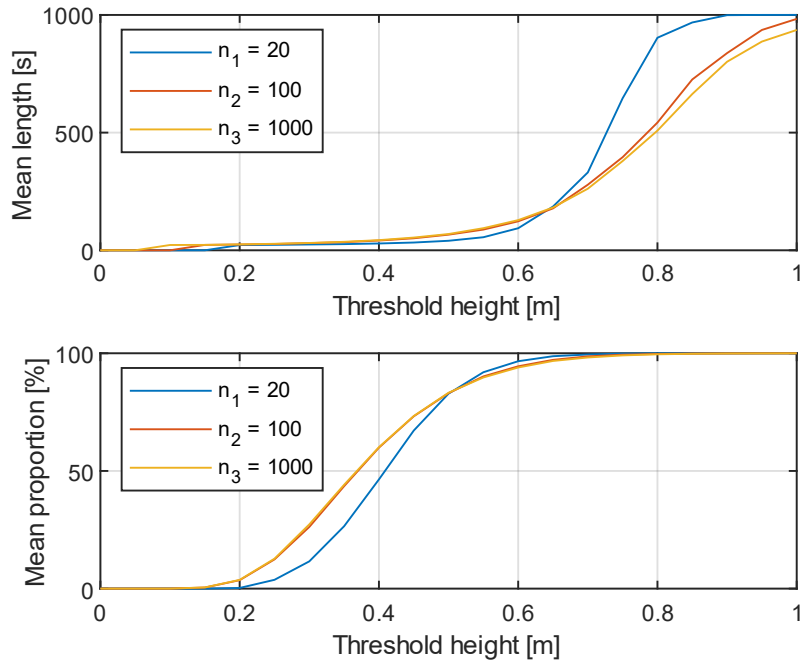
Figure 6: Mean length and mean total proportion of QPs in the signal

For a threshold height of $0\,m$, there is obviously no QP. On the contrary, when A_{max} is high there is only a few chances for a wave to be higher and the whole signal is detected as quiescent. The mean length of QPs comes close to the total length of the signal which is $T_{max} = 1,000\,s$ here.

The interesting threshold range corresponds to a realistic proportion of QPs, namely when this ratio is lower than $50\,\%$, as it can really be called a quiescent period. Figure 7 zooms in the pertinent range of thresholds.
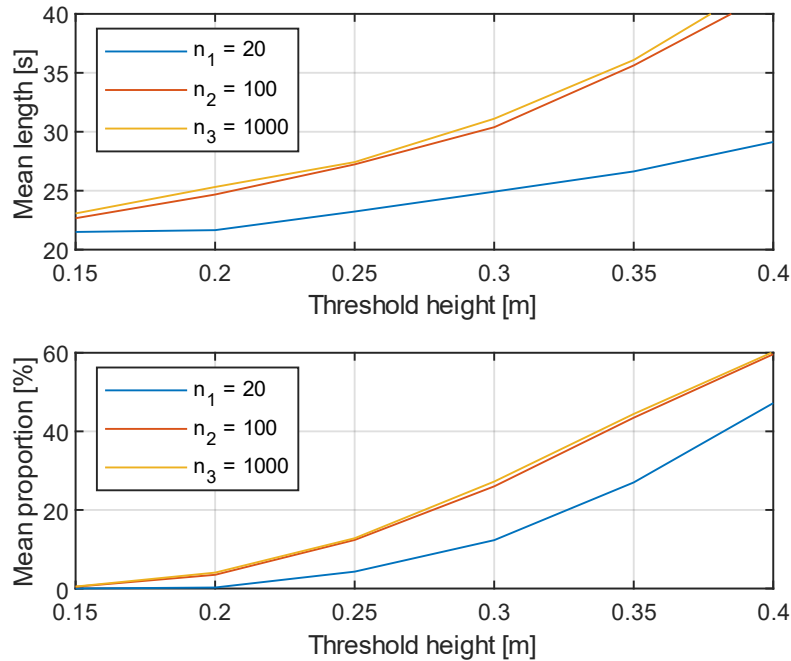
Figure 7: Mean length and total proportion of QPs for the pertinent threshold range

We clearly notice that the proportion and mean length of QPs in the signal composed by $n_1 = 20$ components are lower than for n_2 and n_3. A higher discretization confirms the convergence of those properties for large values of n, $n_3 = 1,000$ being very close to the infinite case. Hence, the statistical properties of this signal are similar to the properties of an infinite sum of cosines.

Figure 8 reveals additional information on the length distribution of the quiescent periods. An arbitrary threshold height of $0.3\,\mathrm{m}$ was used; the distribution of QPs length is similar for different values of A_{max}.
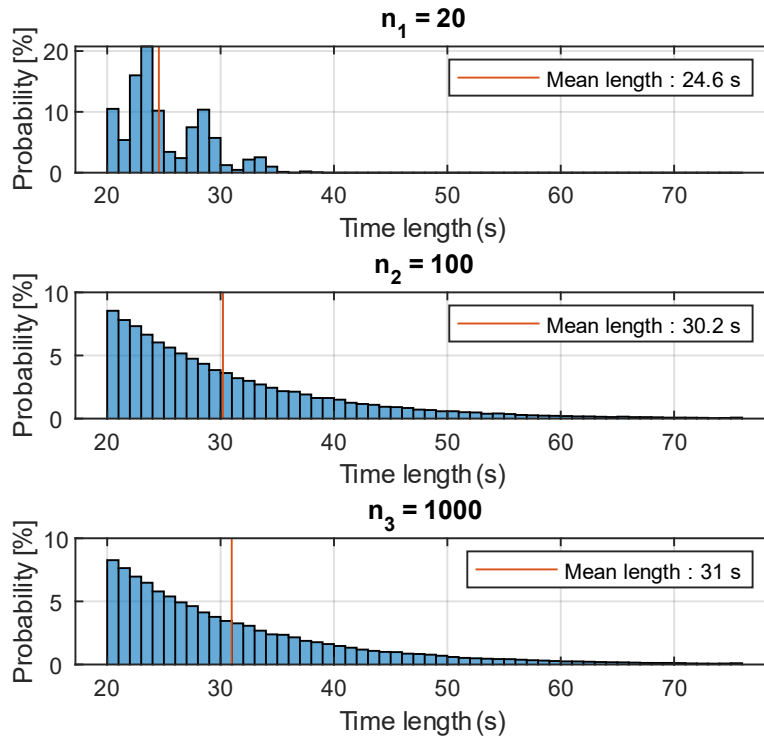
Figure 8: Quiescent period length distribution

The high periodicity of the first signal leads to uneven distributed QPs lengths. For the two other signals, the probability to find QPs of a certain time length follows a logarithmic decrease. In Al-Ani et al. (2019), this property is also highlighted.

We can also study the influence of the parameter T_{min} on the mean length of QPs. Figure 9 shows the mean length and proportion of QPs for various values of T_{min}. Only the case $n_3 = 1,000$ is displayed here.
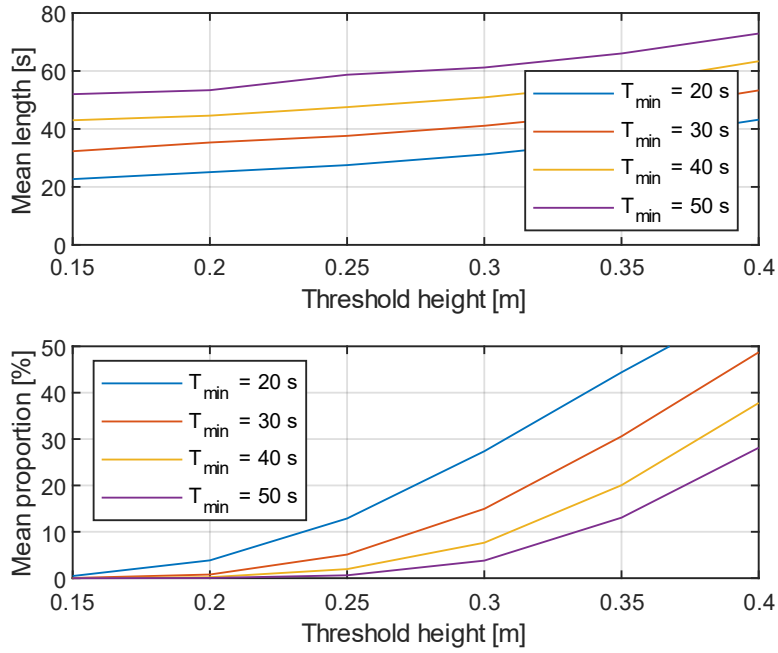
Figure 9: Mean length and total proportion of QPs for different minimum QP lengths

An interesting property of QPs can be highlighted: for a given threshold, the difference between the mean length T_{QP} and the minimum time T_{min} of QPs is independent from this parameter T_{min}. A deeper look into this property would be interesting, but no explanation has been found yet using the distribution of QPs length.

Figure 10 displays this difference for several values of T_{min}. This property allows us to use only one value of T_{min} to compute the mean length of any QP. However, the total proportion of QPs in the signal depends on T_{min}. Consequently, we need Figure 10 to find all useful statistics.
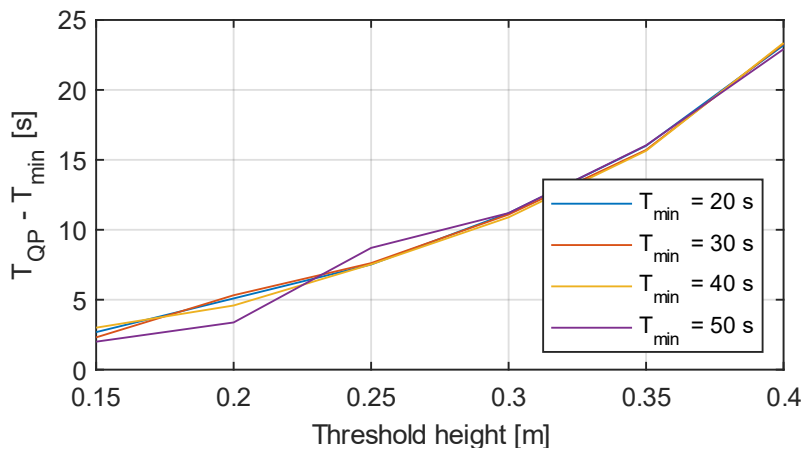
Figure 10: Difference between the mean time and the minimum length of QPs

Figure 9 allows us to find precious information about the quiescent periods that we could find in a sea state close to the ideal conditions described by the JONSWAP spectrum. To illustrate this, let us consider a helicopter landing on a vessel, in a large sea state defined by $H_s = 3.8\,\text{m}$ and $T_p = 8\,s$ being possible real conditions. The maximum wave height from trough to crest is limited to two meters during the landing for safety measures, which means that the threshold height is set to $A_{max} = 1\,\text{m}$. The pilot needs a time window of at

least $T_{min} = 25$ s to perform the operation. Only the case $n_3 = 1,000$ components is considered here.

First, we need to scale these data to fit the computed graphs. The values corresponding to the real sea state will be denoted r ($H_s^r = 3.8$ m and $T_p^r = 8$ s), and the values corresponding to the reference scaled sea state will be denoted s ($H_s^s = 1$ m and $T_p^s = 10$ s). The scaled threshold height is then:

$$A_{max}^s = A_{max}^r \cdot \frac{H_s^s}{H_s^r} = 1 \cdot \frac{1}{3.8} \simeq 0.263 \text{ m,}$$

(5)

and the scaled minimum length of QPs is:

$$T_{min}^s = T_{min}^r \cdot \frac{T_p^s}{T_p^r} = 25 \cdot \frac{10}{8} = 31.25 \text{ s.}$$

(6)

For these scaled values, Figure 9 gives the mean length and proportion of QPs longer than T_{min}^s in the scaled state: $T_{QP}^s \simeq 39$ s and $P_{QP} \simeq 5\,\%$. In the real sea state, the mean length of these QPs is:

$$T_{QP}^r = T_{QP}^s \cdot \frac{T_p^r}{T_p^s} = 39 \cdot \frac{8}{10} = 31.2 \text{ s.}$$

(7)

3.2 Mean gap and waiting time between quiescent periods

These results are extremely useful for decision-makers. With the mean QP length and proportion of QPs in the signal, we can compute the mean gap between two succeeding QPs. This gap corresponds to the time interval separating the end of a QP from the start of the following one. This mean gap is given by:

$$T_{gap} = \frac{T_{QP}}{P_{QP}} - T_{QP}$$

$$= \frac{31.2}{0.05} - 31.2 \simeq 593 \text{ s} \simeq 10 \text{ min.}$$

(8)

We remark that this gap is long for the example above: this is mainly due to the low occurrence of QPs, with only $5\,\%$ of the signal covered by QP intervals. We can also compute the mean interval between the start of a QP and the start of the following one, which is simply:

$$T_{interval} = T_{gap} + T_{QP} = \frac{T_{QP}}{P_{QP}}.$$

(9)

Another quantity of interest is the mean waiting time for a quiescent period to occur. This notion refers to the mean time that one has to wait to find the start of the first incoming QP from a random point in time. In real life conditions, when someone decides to perform an operation from a starting point, this waiting time corresponds to the mean time he/she has to wait before being able to start the manoeuvre. The mean waiting time is given by the expression:

$$T_{WT} = \frac{T_{min}}{2} + \frac{T_{gap}^2}{T_{interval}} = \frac{T_{min}}{2} + P_{QP} T_{QP} \left(1 - \frac{1}{P_{QP}}\right)^2 = \frac{T_{min}}{2} + T_{gap}(1 - P_{QP}).$$

(10)

This formula was found by fitting the real waiting time (obtained from direct computation) and the waiting time obtained from the previous statistics. Despite intensive discussion

and thinking with my supervisor and colleagues, no precise mathematical explanation could be given.

Figure 11 shows the mean gap, interval and waiting time for the scaled sea state of reference, with $T_{min} = 2T_p = 20$ s. Overall, the three quantities are close to each other, but we always have:

$$T_{WT} < T_{gap} < T_{interval}. \tag{11}$$
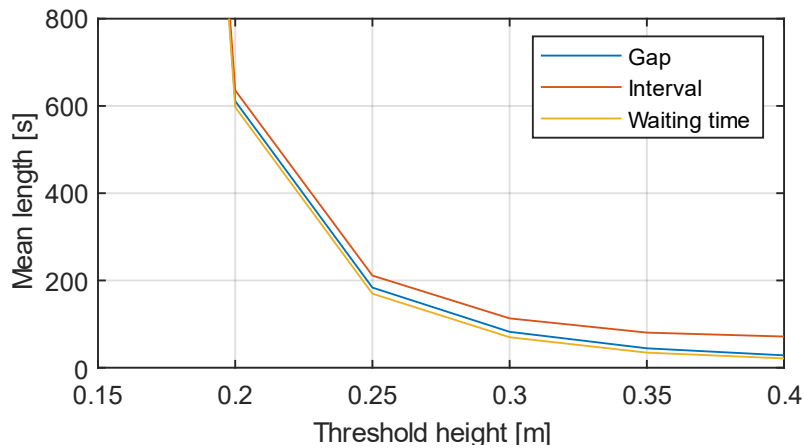
Figure 11: Mean gap, interval and waiting time between two QPs

The gap and waiting time increase exponentially when the threshold decreases: for a threshold of 0.15 m, they are close to $4,000$ s. Last, we can compute the mean waiting time for different values of T_{min}, as illustrated in Figure 12: the mean waiting time increases significantly with T_{min}. We observe that for QPs of at least 30 seconds and thresholds below 0.2 meters, the waiting time goes to infinity: a marine operation cannot be performed for these parameters.
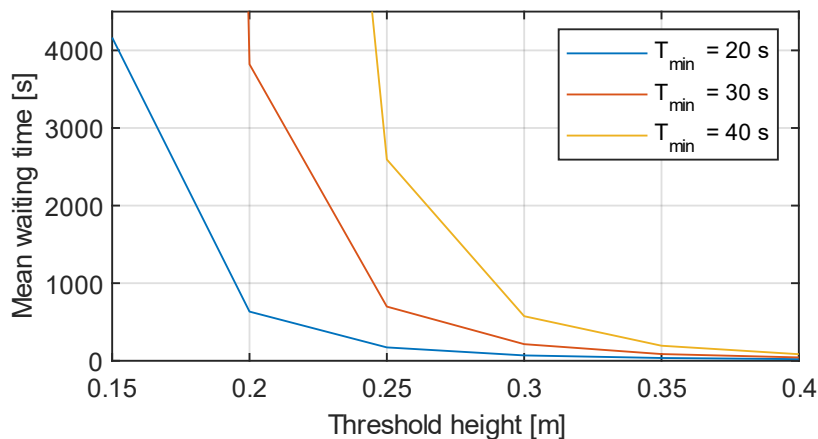
Figure 12: Mean waiting time for different values of the minimum QP time

If one wants to use these graphs to extract the statistics previously presented, scaling the data to fit the reference JONSWAP parameters is the only required step. These quantities can help decide if the desired parameters for a marine operation are coherent with the current sea state, and if the probability to find a quiescent period in a close future is high enough.

3.3 Statistics of quiescent periods for vessel motions

It is possible to extract the same statistics for the quiescent periods that can be found in the motions of a ship that navigates in a given sea state. In this section, only the case $n_3 = 1,000$ is considered, with the reference sea state given by $H_s = 1$ m and $T_p = 10$ s.

The equivalent of Figure 9 for the vessel motions is presented in Figure 13: it shows the mean length and mean proportion of QPs in each motion, for the pertinent range of thresholds and different minimum times. The motion statistics are very similar to the wave statistics, only the threshold range differs. We can use it to extract the useful statistics for the motions, such as the mean length and proportion of QPs of a certain minimum length, as well as the average waiting time and gap between two successive QPs.

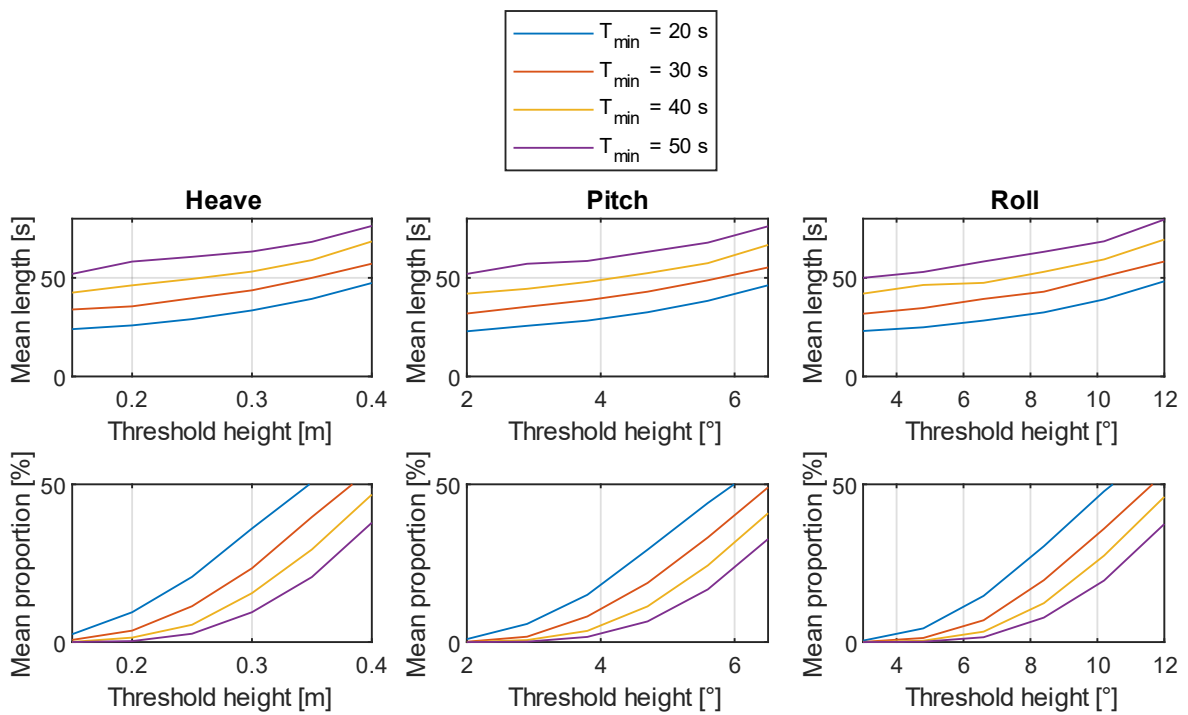**Figure 13: Mean length and total proportion of QPs for the vessel motions for different minimum QP times**

When an operation needs to be performed, we often need all the motions to be calm. Thus, we want to have a look at the QPs that are in common between the different degrees of freedom. Let us consider first the quiescent periods that are in common between heave and pitch, as shown in Figure 14.
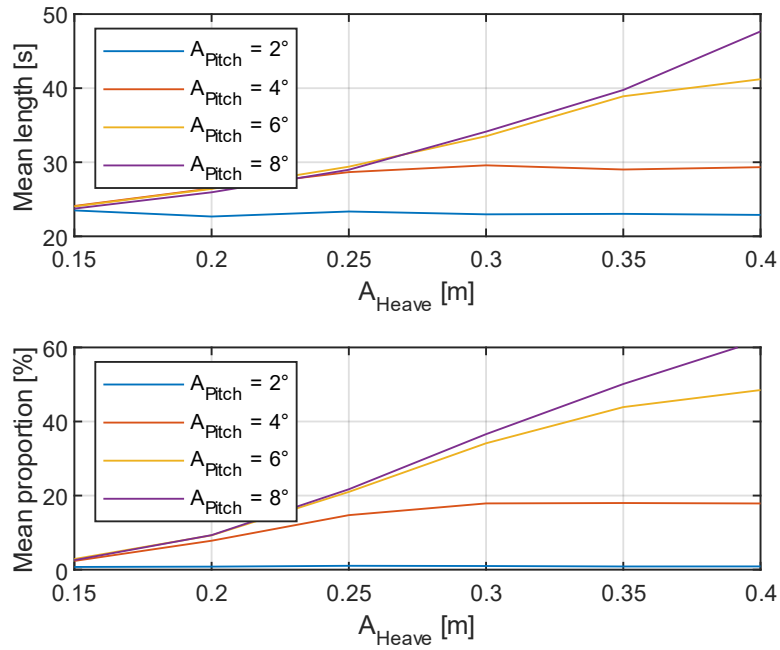
Figure 14: Mean length and total proportion of QPs that are in common between heave and pitch

A few comments can arise. To start with, the curve corresponding to the lowest threshold height for pitch is constant. The most restrictive parameter is the pitch threshold, and almost every QP that is detected for pitch is also detected for heave. On the contrary, the highest pitch threshold is not restrictive and we find the curve for heave only. When the threshold heights are balanced between the motions, both can be restrictive and the proportion of QPs is lower than for only one degree of freedom. The same data is shown in Appendix 2 in a three-dimensional way. The same computation can be done for QPs in common with heave and roll or pitch and roll; the results are similar.

Last, we can fix the threshold heights of the three degrees of freedom, and study in which way finding QPs that are in common for the three motions restricts their occurrence. Several cases can be found:

- The occurrence of QPs is similar for the three motions: the three threshold heights are equally restrictive.
- The occurrence of QPs is lower for one of the motions: the corresponding threshold is more restrictive than the others.
- The occurrence of QPs is higher for one of the motions: the corresponding threshold is less restrictive than the others.
- The occurrence of QPs is different for each motion.

The first case is presented in Figure 15 as a function of T_{min}, where the three thresholds are equally restrictive.
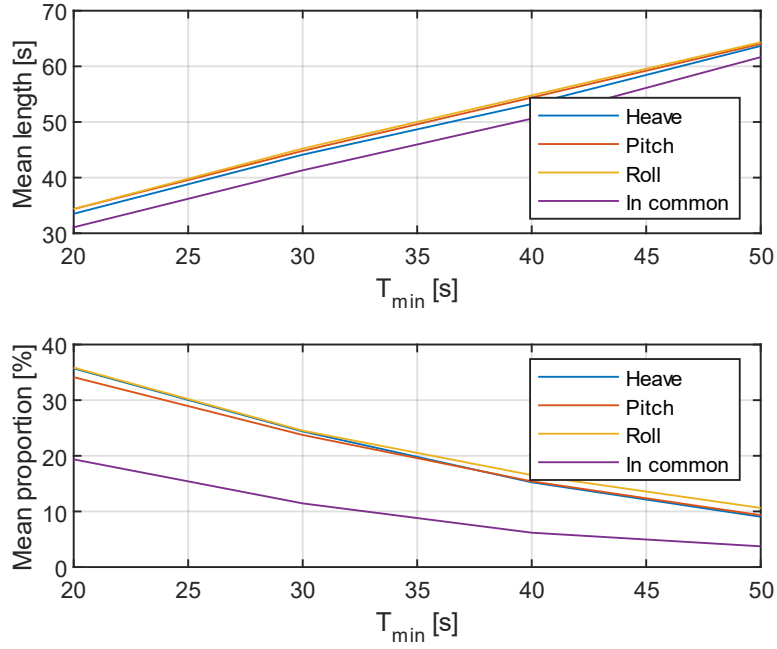
Figure 15: Mean length and total proportion of QPs that are in common between the three motions - equivalent restrictions

The mean length and proportion of QPs is really close for the three motions. The QPs in common between the three motions are about 2 to 3 times less frequent than for each motion, and their length is about 4 seconds shorter. These results show that when carrying out an operation, finding QPs in common between the motions implies significantly longer waiting times and overall shorter QPs. We can use (10) to compute the waiting time of QPs in each motion and in common between the three motions. For instance, for a minimum length $T_{min} = 20\,s$, the waiting times are $T_{WT}^{Heave} \simeq 50\,s$ for heave only and $T_{WT}^{In\,common} \simeq 120\,s$ for QPs in common between heave and pitch.

Figure 16 shows the second case, where the heave threshold was set more restrictive than the pitch and roll threshold heights. The mean length of QPs is similar between the more restrictive motion (heave) and the QPs in common between the three motions. The proportion of QPs in common is lower than in the previous case, and also lower than for heave only: the heave threshold is still not the only restrictive parameter.
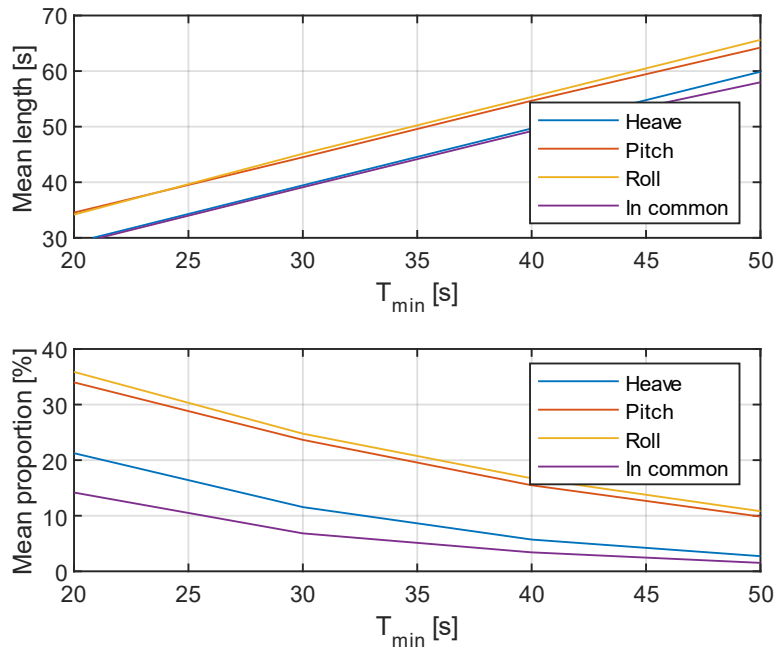
26

Figure 16: Mean length and total proportion of QPs that are in common between the three motions - more restrictive threshold for heave

Analogous comments can be made for the two last cases presented in Appendix 3.

4 Implementation of the Prony method for wave prediction

Invented by Gaspard de Prony in 1795, the Prony method is used for signal filtering and approximation. The powerful Fourier analysis has overshadowed this method for a long time, but the recent improvements in computer technology have made it a useful tool in several engineering applications. The fact that it works correctly for finite time samples sometimes makes it more appropriate than the Fourier analysis, and allows a continuation of the signal that is impossible with the other method. Indeed, the information contained in the Fourier transform is limited to the time window of the original sampled signal, as the inverse Fourier transform is a periodic function of period T_{max}. Attempting a continuation of the signal would lead to a replication of the signal.

This thesis aims at trying this new method and analysing the main parameters that influence the prediction.

4.1 The Prony method

The original method consists in solving two linear systems of equations that lead to the parameters of the solution: damping factors α_k, angular frequencies ω_k, amplitudes A_k and phases φ_k ($k = 1, \dots p$) of the p functions.

It matches a curve $x_p[i]$ of p exponential components to a signal $x_s[i]$ composed of $n_s = 2p$ samples, $x_p[i] \approx x_s[i]$ ($i = 1, \dots n_s$) with

$$
\begin{aligned}
x_p[i] &= \sum_{k=1}^{p} A_k \cdot e^{(\alpha_k + j\omega_k) + \Delta t(i-1) + \varphi_k} \\
&= \sum_{k=1}^{p} h_k \cdot z_k^{i-1} \approx x_s[i].
\end{aligned}
\tag{12}
$$

Δt is the sampling period, h_k is the time-independent component and z_k is the exponential component or pole. Here, j is the imaginary unit.

If the p poles are different, equation (12) expresses the general solution of a homogeneous linear difference equation that can be written $\mathbf{Z} \cdot \mathbf{h} = \mathbf{x_s}$:

$$
\begin{pmatrix}
z_1^0 & z_2^0 & \cdots & z_p^0 \\
z_1^1 & z_2^1 & \cdots & z_p^1 \\
\vdots & \vdots & \ddots & \vdots \\
z_1^{p-1} & z_2^{p-1} & \cdots & z_p^{p-1}
\end{pmatrix}
\begin{pmatrix}
h_1 \\ h_2 \\ \vdots \\ h_p
\end{pmatrix}
=
\begin{pmatrix}
x_s[1] \\ x_s[2] \\ \vdots \\ x_s[p]
\end{pmatrix}.
\tag{13}
$$

It has as a characteristic equation

$$
\phi(z) = \prod_{k=1}^{p}(z - z_k) = \sum_{k=0}^{p} a[k] \cdot z^{p-k} \; ; \; a[0] = 1,
\tag{14}
$$

where the poles z_k are the roots of the characteristic polynomial $\phi(z)$ and $a[k]$ are its coefficients.

Equation (12) can be rewritten as a linear prediction model expressed by the following matrix system $\mathbf{T} \cdot \mathbf{a} = \mathbf{x_s}$:

$$\begin{pmatrix} x_s[p] & x_s[p-1] & \cdots & x_s[1] \\ x_s[p+1] & x_s[p] & \cdots & x_s[2] \\ \vdots & \vdots & \ddots & \vdots \\ x_s[2p-1] & x_s[2p-2] & \cdots & x_s[p] \end{pmatrix} \begin{pmatrix} a[1] \\ a[2] \\ \vdots \\ a[p] \end{pmatrix} = - \begin{pmatrix} x_s[p+1] \\ x_s[p+2] \\ \vdots \\ x_s[2p] \end{pmatrix}. \tag{15}$$

$\mathbf{a}$ is called the linear prediction coefficients vector and is made of the coefficients of $\phi(z)$. $\mathbf{x_s}$ is the observation vector, and $\mathbf{T}$ is the forward linear prediction matrix (a Toeplitz matrix).

The Prony method is structured in three main steps:

1. Solving the linear system (15) to get the values of $\mathbf{a}$ that are the coefficients of the characteristic polynomial $\phi(z)$.
2. Finding the roots z_k of $\phi(z)$, leading to the damping factors and frequencies:

$$\alpha_k = \frac{\ln|z_k|}{\Delta t}, \tag{16}$$

$$\omega_k = \frac{\tan^{-1}\left[\frac{Im(z_k)}{Re(z_k)}\right]}{\Delta t}. \tag{17}$$

3. Solving the original system (13) to get the values of $\mathbf{h}$, that lead to the amplitudes and phases:

$$A_k = |h_k|, \tag{18}$$

$$\varphi_k = \tan^{-1}\left[\frac{Im(h_k)}{Re(h_k)}\right]. \tag{19}$$

This method is used when $n_s = 2p$, and results in an exact fit between the sampled signal and the exponentials if matrices $\mathbf{T}$ and $\mathbf{Z}$ are non-singular. When $n_s \neq 2p$ which is often the case, the two systems are either overdetermined (more equations than unknowns) or underdetermined. The solutions can be approximated via different methods, such as the least squares (LS) or the total least squares (TLS) methods.

The least squares approach gives a solution to the general minimization problem $\min\|\mathbf{Ax} - \mathbf{b}\|$, with $\mathbf{A} \in \mathbb{C}^{m,n}$, $\mathbf{b} \in \mathbb{C}^{m,1}$, $\mathbf{x} \in \mathbb{C}^{n,1}$. The solution is given by the normal equation:

$$\mathbf{x}_{LS} = (\mathbf{A}^H\mathbf{A})^{-1}\mathbf{A}^H\mathbf{b}, \tag{20}$$

where H denotes the Hermitian conjugate of a complex matrix. In practice, MATLAB computes the least squares solution with its own algorithms, using more efficient methods based on QR or LU decomposition.

The Prony analysis results in the p exponential components that are summed to reconstruct the signal. In practice, it gives both negative and positive frequencies for each component, with the same amplitude, damping factor and phase. In reality, the reconstructed signal is composed of $p/2$ components. In case of an odd number, the first component has a zero amplitude.

4.2 Implementation in MATLAB

In (Fernández Rodríguez et al., 2018), four algorithms are implemented in MATLAB and tested for biomedical signal filtering: the classic method, the LS and TLS methods, and another non-polynomial method called matrix pencil method. The results in this thesis are based on the open access code that is presented in this article. The LS method being the most efficient method, it has been used for wave prediction. The other algorithms have not been tested in this work. After simplification and adaptation of the open access code, the LS algorithm was tested under MATLAB R2022b and is presented in Code 1:

Code 1: Least Squares method for the Prony analysis

```matlab
function [Ap, Alphap, Wp, Phip] = PronyLS (x, p, dt)

    % x: sampled signal to be analysed
    % p: number of components in the reconstructed signal
    % dt: sampling interval

    ns = length(x);      % number of samples

    % Step 1
    T = toeplitz(x(p:ns-1),x(p:-1:1));
    a = -T\x(p+1:ns);

    % Step 2
    c = transpose([1;a]);
    r = roots(c);
    Alphap = log(abs(r))/dt;    % damping factors
    Wp = angle(r)/dt;           % angular frequencies

    % Step 3
    Z = zeros(ns,p);
    for i=1:length(r)
          Z(:,i) = transpose(r(i).^(0:ns-1));
    end
    h = Z\x(1:ns);
    Ap = abs(h);                % amplitudes
    Phip = angle(h);            % phases

end
```

The sampled signal is given in vector x; p is the number of components in the recomposed signal; dt is the sampling interval Δt. The output vectors Ap, $Alphap$, Wp, $Phip$ are the results from the approximation made by the function $PronyLS$.

In step 1, the function $T = toeplitz(c,r)$ creates the Toeplitz matrix from equation (15) of dimensions $(n_s - p) \times p$ ($p \times p$ in the classic method), with c as its first column and r as its first row. The system is then solved with the computation of **a**. The MATLAB backslash operator is used to solve linear systems of the form $\mathbf{Ax} - \mathbf{b}$. In the case of square matrices, $\mathbf{A}\backslash\mathbf{b}$ computes the matrix $\mathbf{A}^{-1}\mathbf{b}$ if $\mathbf{A}$ is invertible. For non-square matrices, it returns a least squares solution of the system.

The coefficients of the polynomial $\phi(z)$ are now found. In step 2, the function $r = roots(c)$ obtains the roots of this polynomial defined by the row vector c. This vector must also contain the element $\mathbf{a}[0] = 1$, which was not obtained in the system solution and is added to vector **a**. With the obtained roots r that correspond to z_k in the problem to solve, the damping factors and frequencies can be computed with equations (16) and (17). The MATLAB function $angle(r)$ computes the phases of the roots.

Step 3 starts with the creation of the matrix $\mathbf{Z}$ from the original system $\mathbf{Z} \cdot \mathbf{h} = \mathbf{x_s}$ (of dimensions $p \times p$ in the classic method and $n_s \times p$ in the least squares method). The system is then solved to obtain $\mathbf{h}$, which leads to the amplitudes and phases from (18) and (19).

4.3 Predictions based on least squares Prony method

The prediction computations are structured as followed:

- Choice of the original signal parameters: number of components n; number of samples n_s; end time t_1 for the approximation; end time t_2 for prediction; spectrum parameters H_s and T_p.
- Choice of the number of components in the reconstructed signal p from the Prony method.
- Creation of the spectrum and the sampled signal X_s with the random phases model.
- Performing of the Prony analysis on the sampled signal up to t_1.
- Reconstruction of the approximated signal X_p with the obtained frequencies, amplitudes, damping factors and phases up to t_2.
- Comparison of the original and the reconstructed signals along the approximation interval $[0; t_1]$ and the prediction interval $]t_1; t_2]$.
- Calculation of the predicted time τ.

The resolution of the two systems in the Prony algorithm can induce a failure in the analysis, for example if the matrices are rank deficient or singular. This can arise more or less frequently given the parameters of the analysis or the choice of the samples.

An important comment here is that the reconstructed signal X_p is filtered. Sometimes, high frequencies can be associated with negative damping factors. This leads to the explosion of the amplitude after some point. The filtering is simple as we can simply disregard the components with high frequencies, and increases the prediction quality. The cut-off frequency is usually set around $3 \, \text{rad/s}$.

In the least squares approximation, the parameter p must be lower than n_s. In practice, it is easier to consider the fraction $\pi = p/n_s \in \,]0; 1[$. The results of the Prony analysis are given in terms of π. For $\pi = 0.5$, the classic method is used (we have $n_s = 2p$). Otherwise, the least squares method is applied. As it has better results than the classic method (even for $\pi < 0.5$), the value of $\pi = 0.5$ will be avoided in the computations.

Figure 17 shows a signal reconstruction and prediction for two different values of π, for $n_s = 100$ sample points. The black vertical dotted line separates the approximation interval from the prediction interval. This illustrates the different results that the Prony analysis can give: for $\pi < 0.4$, the LS method usually does not obtain a perfect fit with the sampled signal. However, the approximation can be good and give a correct prediction for a few seconds. For $\pi > 0.4$, most of the times the LS method results in a perfect fit as in this example. Here, we could evaluate a correctly predicted time of around 5 seconds.
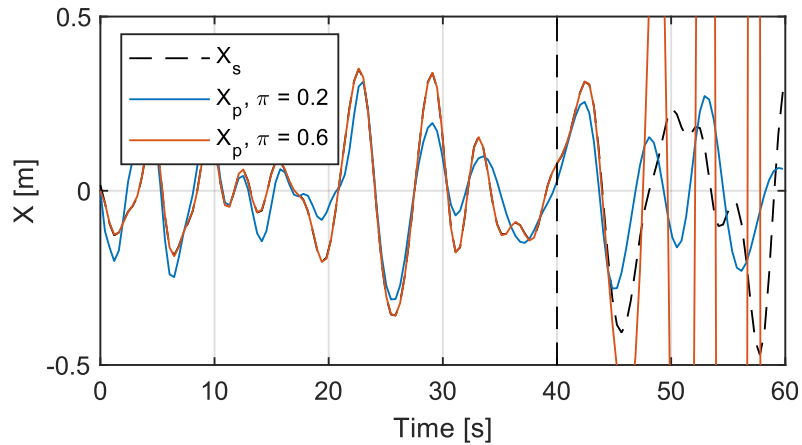
Figure 17: Example of Prony analysis and signal prediction

Figure 18 shows the amplitudes, phases and damping factors plotted as a function of the reconstructed frequencies from the Prony analysis, for the case $\pi = 0.6$ that was presented in Figure 17. Only the positive frequencies are displayed, and the frequencies over 3 radians associated with a zero amplitude are hidden. The approximation of the interval $[0; t_1]$ can be perfect even for completely different components parameters. However, the signals are different after more than five seconds of prediction.
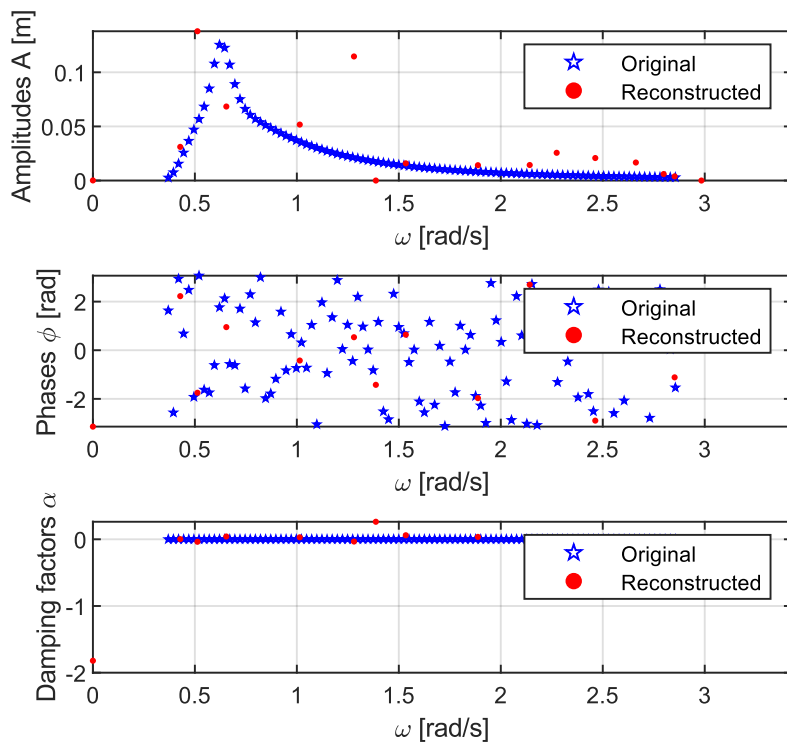

Figure 18: Approximated angular frequencies, amplitudes, phases and damping factors

4.4 Error definition for approximation and prediction

In order to characterise the quality of the approximation and the prediction, we have to introduce an error calculation between the sampled and reconstructed signals. Two different errors are used: the absolute error (AE) and the root mean square error (RMSE).

The AE evaluates the distance between the two signals at any point. The RMSE estimates the average quality of the approximation. They are defined for a time step i by:

$$AE(i) = \left| \frac{x_s[i] - x_t[i]}{M} \right|, \tag{21}$$

$$RMSE(i) = \sqrt{\frac{\sum_{k=1}^{i} \left(\frac{x_s[k] - x_t[k]}{M} \right)^2}{\Delta t \cdot (i-1)}}. \tag{22}$$

For easier comparisons between datasets and later for the vessel motions signals, the signals are normalized by the maximum of the absolute value of $x_s[k]$, $M = \max_{k=1,...n_s} |x_s[k]|$.

First, the quality of the approximation is evaluated by the RMSE at time t_1 for the approximation interval. If this error is below a maximum acceptable error $\varepsilon_{max}^{RMSE} = 0.07$ m, the approximation is qualified as correct enough to be used. In this case, the absolute error and the root mean square error are computed for the prediction part for every time step. The initial point of the RMSE is set at 10 sample points before t_1, so that a bad prediction only for the first samples after t_1 has a smaller influence and gives a chance to the rest. When these errors exceed a maximum acceptable limit ($\varepsilon_{max}^{RMSE} = 0.07$ m and $\varepsilon_{max}^{AE} = 0.2$ m), the predicted signal is considered to be too far from the original one. The final predicted time τ is the average between the predicted times from the absolute error and the root mean square error.

Figure 19 shows an example of a Prony analysis for which $RMSE(t_1) = 0.069$ m: the approximation is barely good enough to be used. Though, the RMSE after t_1 is too high, leading to an overall small predicted time $\tau = 2.4$ s. Appendix 4 shows another example with a perfect approximation, for which the predicted time is $\tau = 7.1$ s.
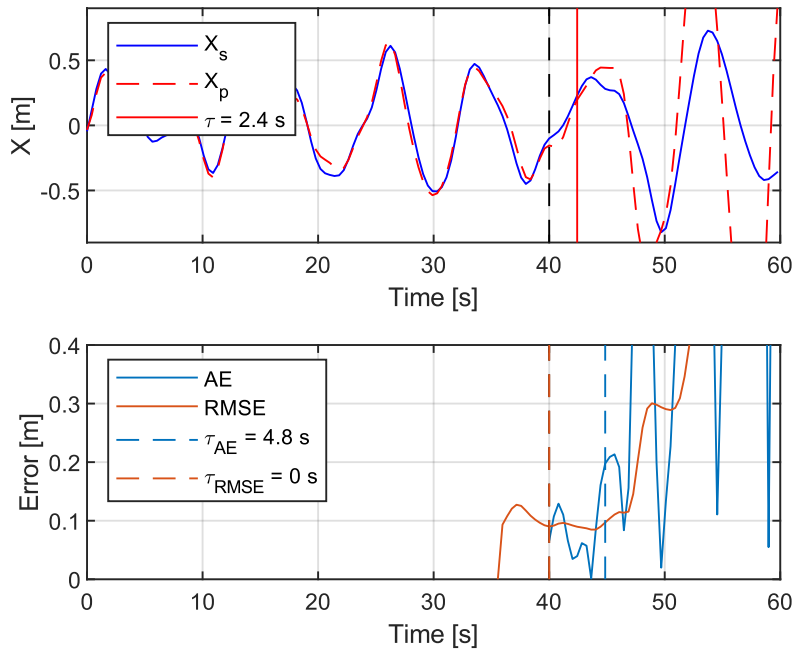

Figure 19: Errors and predicted times on a Prony analysis

5 Parametric study for predictions

The main objective of this section is to study the influence of the parameters that are important for the predictions. Those parameters are:

- n: number of components in the original signal,
- n_s: number of sample points in the original signal,
- t_1: end time for the approximation,
- $\pi = p/n_s$: fraction of the number of components in the reconstructed signal.

The spectrum parameters are not important in this part: stretching the signal in the time or amplitude domains does not influence the scaled predicted time. Thus, all computations are made with $H_s = 1\,\text{m}$ and $T_p = 10\,\text{s}$.

However, one more determining parameter that was studied here is the cut-off frequency that is used to define the spectrum. The effect of the high frequency components in the original signal will be discussed at the end of this section. In the next paragraphs, this cut-off frequency is kept constant: $\omega_{cut} = 2.856\,\text{rad/s}$.

5.1 Number of components in the original signal

First, the influence of the number n of components in the sampled signal is studied. The same numbers from section 3 are used: $n_1 = 20$, $n_2 = 100$ and $n_3 = 1{,}000$. The aim of this study is to find the optimal parameters in terms of prediction quality and success of the analysis.

5.1.1 Low number of components

The main particularity that distinguishes $n_1 = 20$ from n_2 and n_3 is that the associated signal is highly periodic for the time scales considered here. It favours the prediction: it is very easy to find parameters for which the Prony algorithms gives the exact same components as in the original signal, leading to a perfect reconstruction. We need at least $p \geq 2n_1$ to find all original components, as the reconstructed signal is made of $p/2$ distinct exponentials, as explained in 4.1. The time t_1 must be long enough, usually more than $80\,\text{s}$. For example, with $n_s = 200$, $\pi = 0.4$ and $t_1 = 100\,\text{s}$, the Prony analysis results in a perfect reconstruction, with almost one hundred percent success.

For $n_2 = 100$ components, the exact replication of the signal is harder to obtain. In order to find the best parameters for the prediction, we can study the effect of n_s, t_1 and π in a simple optimization process made by hand. First, the limits of the parameters must be defined:

- $n_s \leq 1{,}100$ points: this number is limited by the size of the two systems to solve. For higher numbers, the analysis is unstable and often fails.
- $\pi \geq 0.35$: the results are particularly bad for lower values.
- $100 \leq t_1 \leq 500$: the results are bad for lower values, and the sampling quality is not correct for longer time lengths. For a smooth enough signal, the maximum sampling interval should not be longer than $\Delta t_{max} = 0.5\,\text{s}$. Thus, we consider $t_1 \leq \Delta t_{max} \cdot n_s$.

Once the limits are defined, we can run a set-based optimization process. The visualization of the results is easier when only two parameters vary. The following figures highlight the results of the computation. Each point is an average calculated on 200 iterations.

First, Figure 20 shows the predicted time as a function of π and n_s, as well as the proportion of successful analyses. t_1 was fixed with a value of 200 s. The curve for $n_s = 200$ points is considered irrelevant as $\Delta t = 1$ s, but is still displayed for comparison. For $n_s \geq 500$, the predicted times are equivalent, with a maximum for $\pi = 0.45$ and $\pi = 0.55$ of almost 12 seconds of average predicted time. The analyses are more successful for larger values of π, but the predicted time decreases. $\pi = 0.85$ could also be considered, as it has a really high success rate. This rate is also slightly higher when the number of sample points is low.
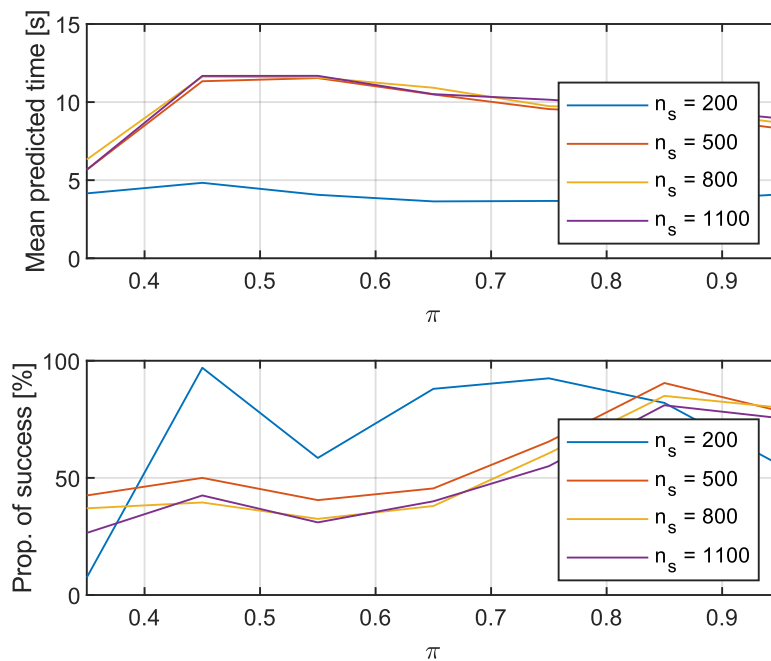

Figure 20: Prediction quality as a function of the number of exponential components and number of sample points, for 100 components in the original signal

Figure 21 then shows the same quantities as a function of the number of sample points and the end time for the approximation interval. The value of $\pi = 0.45$ was used here. We should keep in mind that these curves are relevant when $t_1 \leq \Delta t_{max} \cdot n_s$: for $t_1 = 500$ s, only $n_s \geq 1{,}000$ should be kept. For $t_1 = 300$ s, only $n_s \geq 600$ should be considered. We notice that for $t_1 = 500$ s, the average predicted time is 20 s, which is in reality the prediction end time. This means that the approximation is perfect and the components are the same as in the original signal. However, due to the substantial size of the systems to solve, the rate of success is lower than $30\,\%$: the Prony analysis either results in a perfect reconstruction or in a failure most of the time.
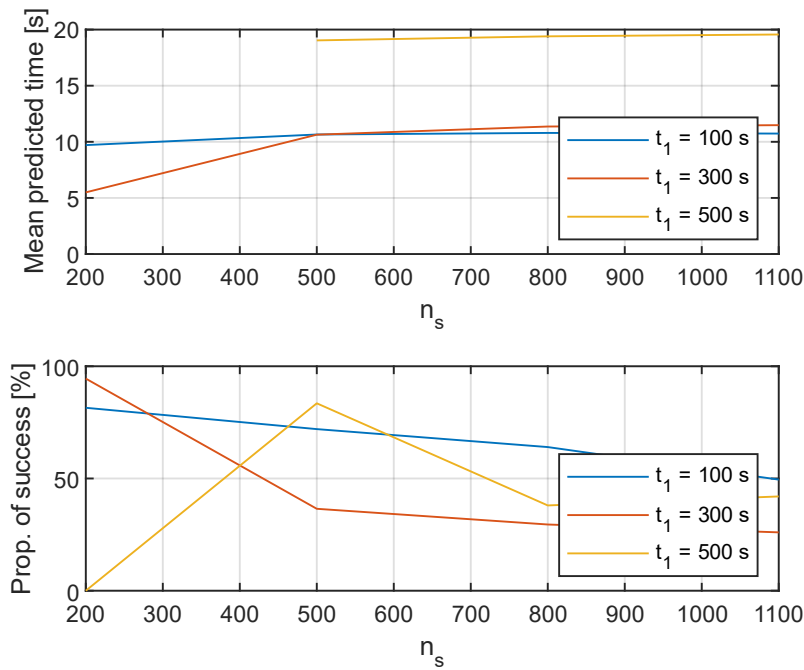
Figure 21: Prediction quality as a function of the number of sample points and the approximation end time, for 100 components in the original signal

Appendix 5 shows the same computation for $\pi = 0.85$. The average predicted time is similar to the previous case, except for $t_1 = 500\,\text{s}$ for which there are no perfect reconstructions. Nonetheless, the success rate is much higher. We globally see an increased prediction time for higher numbers of sample points.

To complete these two figures, we can also plot the prediction quality as a function of π and t_1, also shown in Appendix 5. It confirms the previous comments. The best average predicted time is around 12 seconds, and is obtained by a wide range of parameters values.

5.1.2 High number of components

In the last case $n_3 = 1,000$, the Prony analysis cannot result in a perfect approximation due to the size of the systems. This case is the closest to an infinite number of linear components in the case of an irregular sea state. The same optimization process was made in order to find the best parameters and assess the quality of the Prony predictions.

For simplicity, only the case $t_1 = 300\,\text{s}$ is studied. As no perfect approximations can be obtained, this value achieves good results both for the predicted time and the success rate. Figure 22 shows the prediction quality as a function of π and n_s. The results are very similar to the previous case $n_2 = 100$ components. The best average predicted times are around 12.2 seconds, obtained for $\pi = 0.45$, and $n_s = 800$ or $1,100$. However, the success rate is very low, with around 20 % of correct approximations. This rate is significantly higher for high numbers of components in the reconstructed signal, $\pi = 0.85$ being again a value of interest with an average predicted time of 10 seconds but 80 % of success.
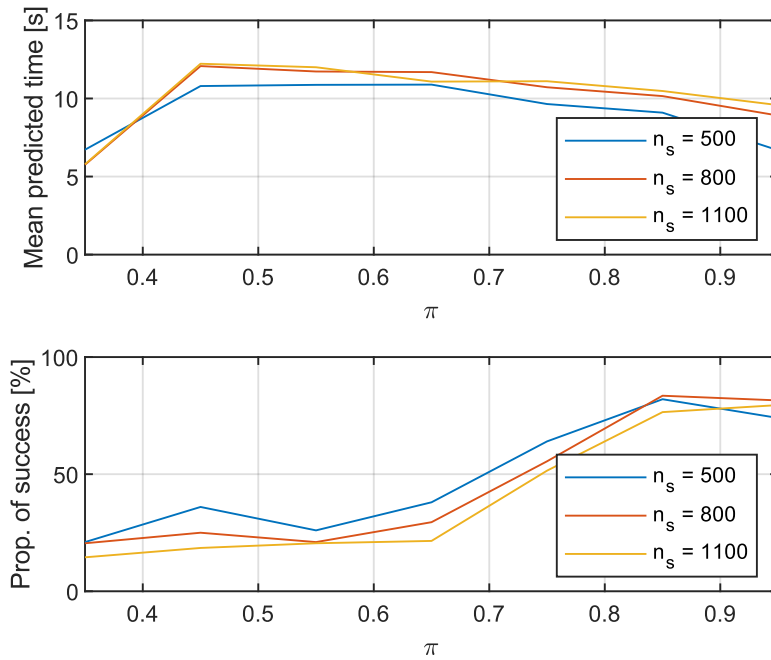
Figure 22: Prediction quality as a function of the number of exponential components and number of sample points, for 1,000 components in the original signal

For complementary information on the predicted times, Figure 23 displays the distribution of the predicted times τ for the case $\pi = 0.45$, $n_s = 1,000$ and $t_1 = 300\,\text{s}$, computed for 1,000 iterations. The average predicted time μ and the standard deviation σ are specified. 98 % of analyses obtain more than 7.5 seconds of prediction: this proves that when the approximation is successful, in other words the RMSE for the approximation part is below the maximum acceptable error, the Prony method is totally reliable for this time interval.
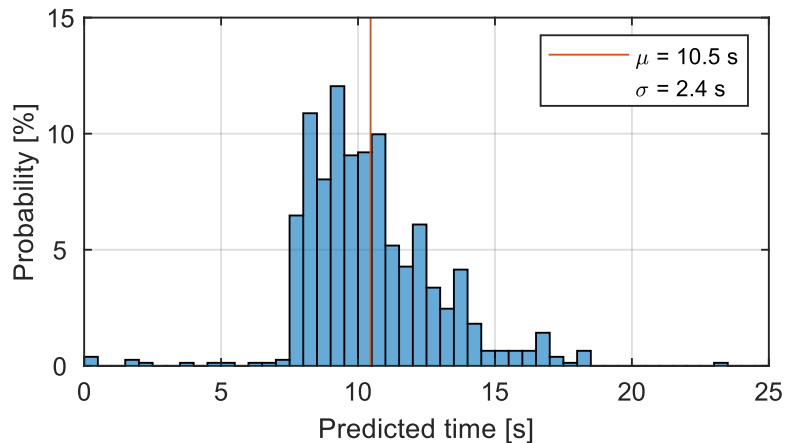

Figure 23: Predicted time distribution for the waves

5.2   Motion prediction

The performances of the Prony analysis for wave prediction were analysed in the previous part, with a few seconds or consistent predictions. But marine operations often require more than 30 seconds of quiescence to be performed. This part focuses on vessel motions predictions. It aims at evaluating the effect of the transfer functions on the prediction quality.

The same transfer functions as in section 3.3 are used for heave, pitch and roll. The errors definition and restrictions are similar than in the previous part. Only the case $n_3 = 1,000$ components is studied here, as it is more reflective of a real case.

First, one should keep in mind that the success of the Prony analysis is often low: obtaining a correct approximation for the three motions at the same time is really rare. Thus, the statistics that are presented here are computed independently for each motion. This can also be a determining factor when using the Prony method for marine operations: it might be easier to predict waves and use a motion model on the predicted signal than first computing the motions and using the Prony tool on the obtained signals.

The short optimization process of the previous section is repeated for the motions. Prediction quality is presented in Figure 24 as a function of π and n_s, for a fixed $t_1 = 300\,\text{s}$. The predictions are slightly better, with 15 to 17 seconds in average. The success rates are equivalent to the waves case. We observe the same optimal parameters as previously: the Prony analysis works the same way for the motions than for the waves. One explanation for the longer predictions would be that the transfer functions act as filters, reducing the high frequency noise.
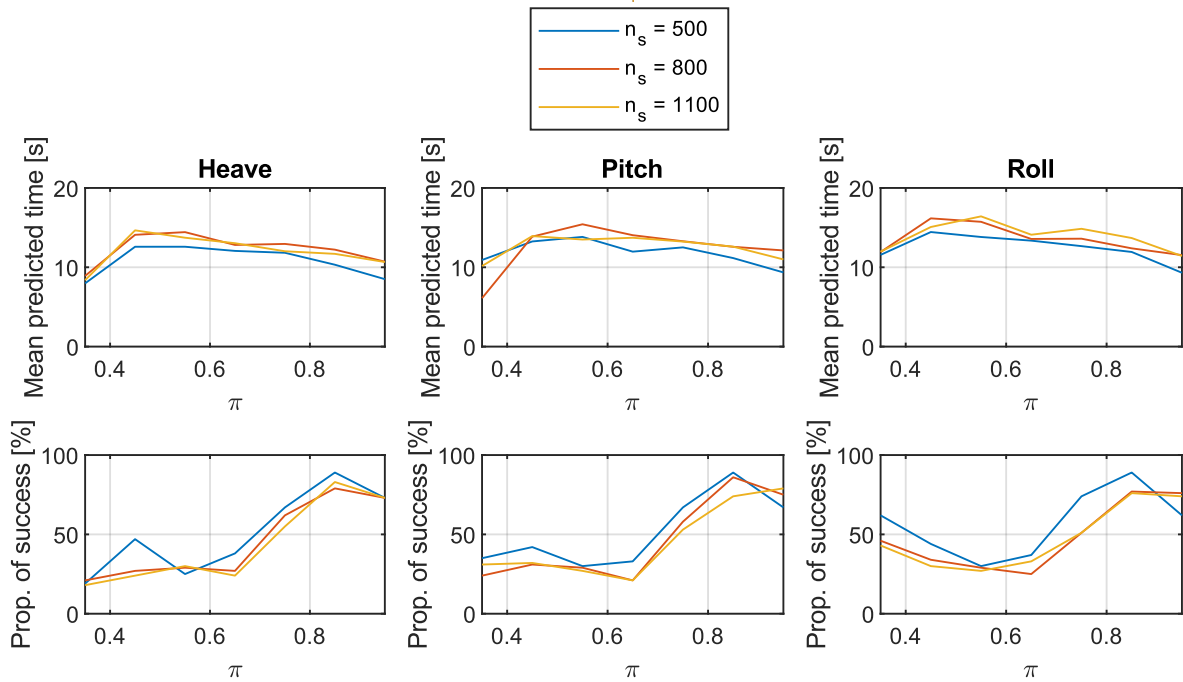

Figure 24: Prediction quality as a function of the number of exponential components and number of sample points, for the vessel motions

5.3   Signal filtering for longer predictions

The better predictions obtained for vessel motions arise the question of high frequency noise and signal filtering. To my knowledge, the impact of a signal filtering preceding the Prony analysis has not been studied yet.

The sampled signal is created via a random phases model, and consists of a sum of sinusoidal components. The filtering is thus done simply, by removing every component with a frequency $\omega > \omega_{cut}$. In the case of real data, a low-pass filter would give similar results. The original signal is created with $n = 10,000$ components, for $\omega_{cut} = 4\,\text{rad/s}$. For $\omega_{cut} = 1\,\text{rad/s}$, about $83\,\%$ of the components are removed (the signal contains exactly $n = 1,736$ components). The previous parts and some tests have shown that for $n > 1,000$

components, the results are independent from this number n: the effect of filtering is only reflected in the removal of high frequencies.

Consequently, there are now two filtering steps for the predictions. First, a preliminary filtering of the wave signal removes the high frequencies before the computation of the motions and the Prony analysis. This section will analyze the impact of this filtering. After the analysis, a second filtering process is carried out, this time on the reconstructed signal. This filtering is only performed to get rid of the high frequencies associated with positive damping factors, which otherwise would lead to a divergence of the reconstructed signal. For this second filtering, the prediction is untouched when the signal does not diverge. The choice of this second cut-off frequency is not important and can be kept constant, for example around $4\omega_p$.

Only two cases for the parameters of the Prony analysis are analysed here: $n_s = 1,000$ sample points; $t_1 = 300\,s$; for $\pi = 0.45$ and $\pi = 0.85$. In the previous study, these two cases obtained very good results. Figure 25 shows the first case, for $\pi = 0.45$ which obtains the best results regarding the predicted times. Appendix 6 presents the second case, that has a much higher success rate but slightly shorter predictions.
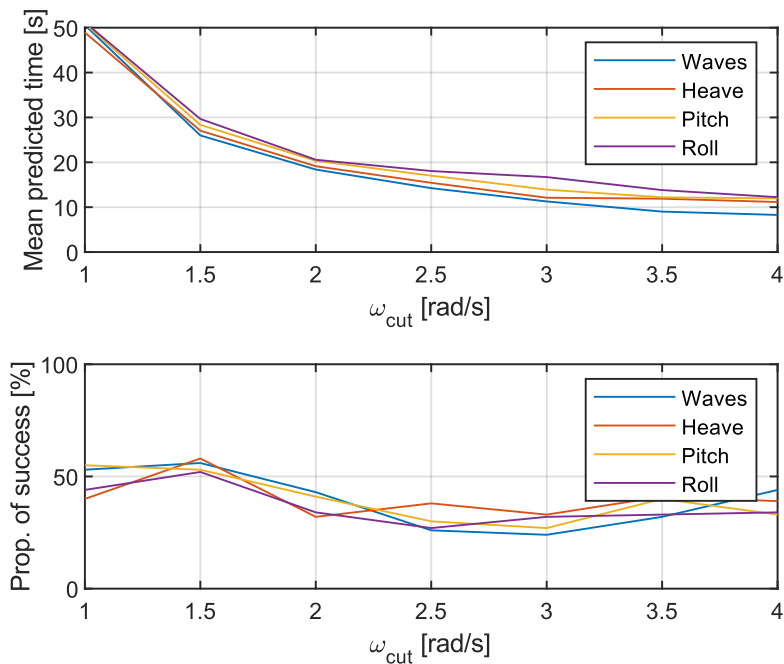

Figure 25: Influence of high frequency filtering on the prediction quality

The filtering has a strong impact on the prediction quality. First, the chance of success of the analysis is slightly higher for lower cut-off frequencies. Second, we observe a clear increase of the average predicted times, up to 50 seconds for $\omega_{cut} = 1\,\mathrm{rad/s}$. However, there is a need to define the minimum acceptable cut-off frequency so that the filtered signal still reflects the original one.

This is presented in Figure 26 where the wave and heave signals have been filtered with cut-off angular frequencies of $2\omega_p = 1.26\,\mathrm{rad/s}$ and $3\omega_p = 1.89\,\mathrm{rad/s}$. The wave signal is slightly modified for $\omega_{cut} = 2\omega_p$. As the transfer functions already act as filters, the heave signal stays really close to the non-filtered one. Thus, we can consider that a cut-off frequency of $2\omega_p$ is acceptable for the ship motions. For waves only, it might be more realistic to have a larger cut-off frequency such as $3\omega_p$.
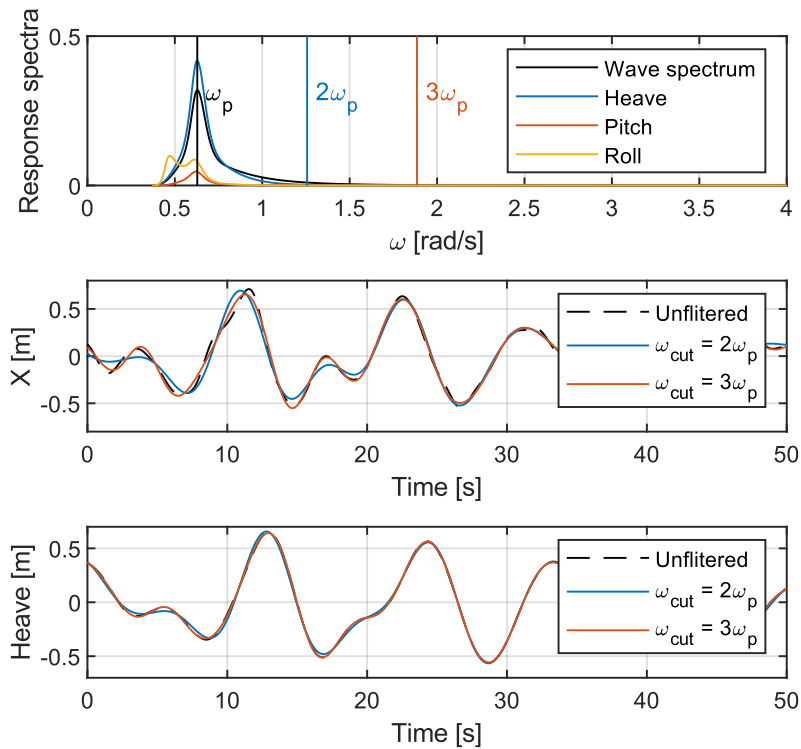
Figure 26: Filtration of the wave and heave signals

We can then use Figure 25 to check the best average predicted time that is associated with these cut-off frequencies: for the waves with $\omega_{cut} = 3\omega_p$, the mean predicted time would be around 20 seconds. For the motions with $\omega_{cut} = 2\omega_p$, this time would be around 35 seconds, which is twice longer than without filtering. For large vessels with slower motions and in other sea states, this time could be even greater and the Prony method might achieve predictions of one minute.

For complementary information, Figure 27 shows the predicted times distribution for the vessel motions, in the case $\omega_{cut} = 3\omega_p$ for the waves and $\omega_{cut} = 2\omega_p$ for the motions. The parameters of the Prony analysis are $n_s = 1,000$ sample points, $t_1 = 300$ s, $\pi = 0.45$. The worst analyses for the motions obtain 20 seconds of prediction, and 95 % of them achieve predicted times of at least 28 seconds (30 seconds for roll), which gives a large reliable window for the Prony method predictions. In the case of the waves, this window is not as large, reaching 17 seconds, because the cut-off frequency is set higher.
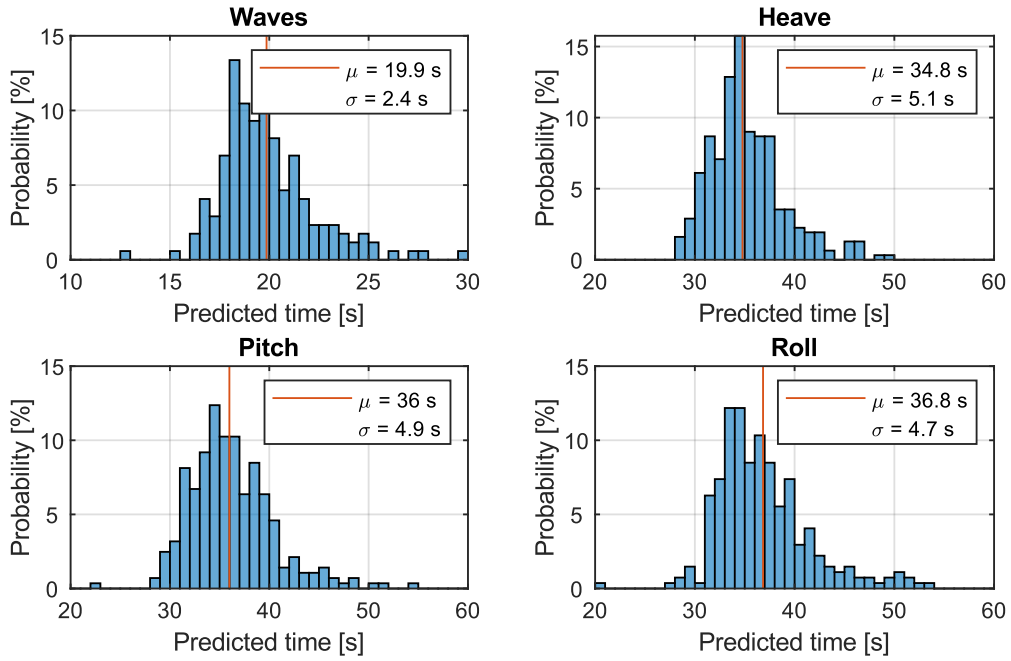
Figure 27: Predicted times distribution after filtering

Figure 28 shows an example of waves and motions signals that are all correctly predicted at the same time, which is rare for the same parameters as in Figure 27, as the success rate is low.
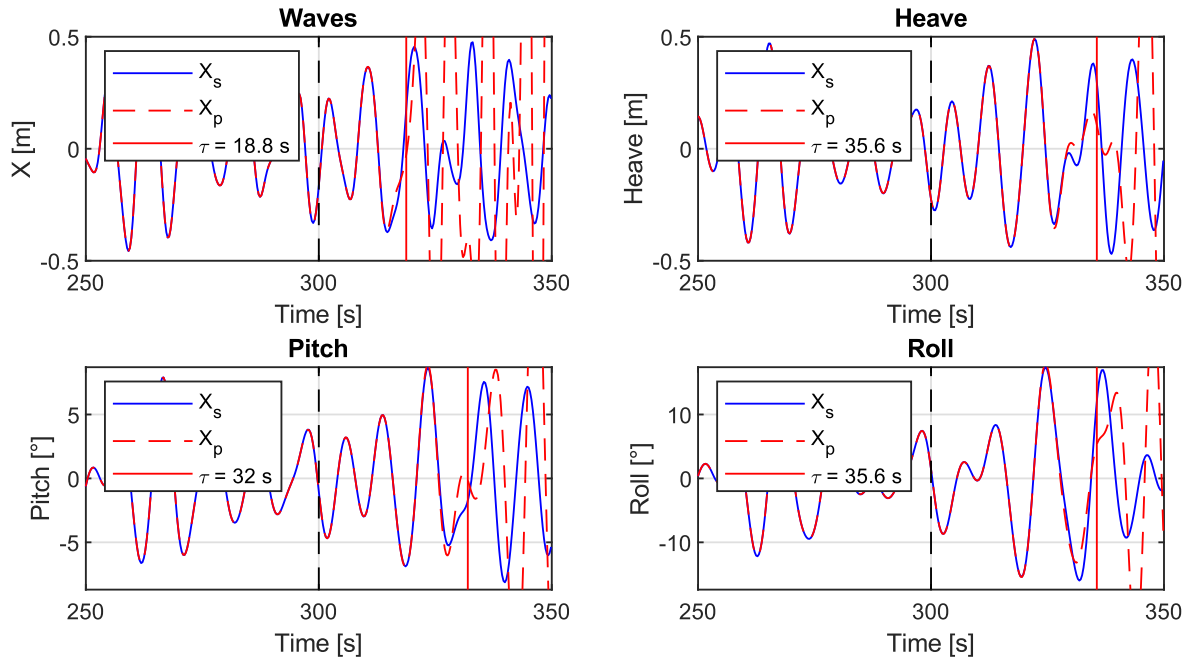

Figure 28: Example of four successful predictions with the optimal parameters

Last, the question that arose was whether the error was related to the quality of the predictions or if these quantities were independent. It appears that for the values of $\pi > 0.4$, the Prony analysis results either in a perfect approximation of the sampled signal or in a failure of the method, with a very few exceptions. This is shown in Figure 29 for 200 attempts. The computation parameters are similar to those used in Figure 27.
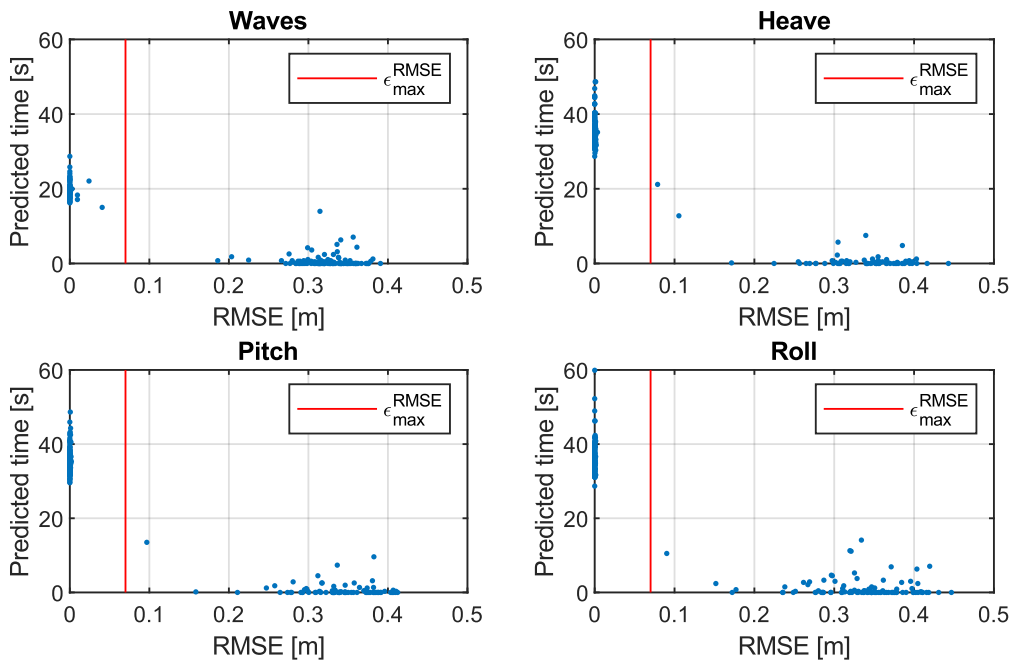
Figure 29: Predicted time as a function of the root mean square error

For $\pi < 0.4$, there are no perfect approximations. The RMSE is never zero, but the maximum acceptable errors define the approximations that are good enough. We observe in Figure 30 that in the case $\pi < 0.4$ ($\pi = 0.37$ here), the RMSE for waves is slightly correlated with the predicted time. Only the predictions with $\mathrm{RMSE} < 0.1\,\mathrm{m}$ are shown in the figure. However, the prediction quality being lower than for $\pi > 0.4$, this case is not used. We could set a more restrictive error limit and keep the best approximations, which would lead to better results. However, this would cause the success rate to decrease.
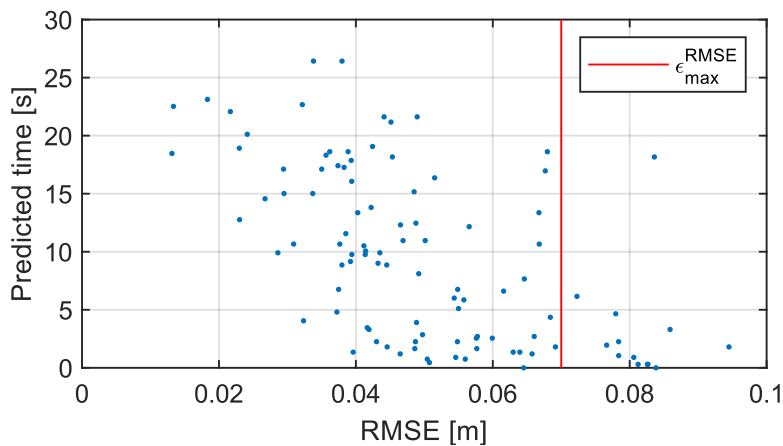
Figure 30: Predicted time as a function of the root mean square error for the waves, for a low number of exponential components

This part showed that filtering the wave signal can significantly increase the prediction quality, without loss of information. For real life applications, the filter must be adapted to the sea state and the quantities at stake, but remains a key parameter of the Prony method.

6 Conclusion

The demand for reliable sea wave predictions used for marine operations leads to an overall improvement of the existing techniques. The real-time methods based on filters now obtain up to fifteen seconds of prediction, while radar imaging combined with wavelet analysis reach two minutes. Up to now, the newly emerged Prony method has mostly been applied to filter design and approximations of ringdown signals, but this thesis is an attempt to use it as a tool for predictions on modelled wave signals.

The main objective of these methods is to detect future quiescent periods which are long enough to perform tasks at sea. In this work, the modelling process of the waves was first explained, and a model for vessel motions was presented. The signals were created via the JONSWAP wave spectrum, used in the linear wave theory in irregular sea states.

Useful quiescent periods statistics were extracted from the signals, showing the distribution of calm intervals and their occurrence rate in the surface elevation and in the motions. Similarities were found with previous work about the logarithmic decrease of the quiescent period distribution with regard to their length. Additional information were added to the previous works, with the average waiting time for such periods to arise. The analysis of these statistics allows for a wise selection of the two main factors affecting the incidence of quiescent periods, namely their minimum length and the maximum amplitude of the signal. These results constitute a planning step that should be completed before applying the prediction method to the waves or the vessel motions.

The theory behind the Prony analysis was described, using the least squares algorithm. It was then implemented for wave prediction in MATLAB, and the method to evaluate the prediction quality was explained.

The last section explored the effect of the important parameters on the predictions. In average, the Prony method obtained accurate reconstructions of 12 seconds for wave signals alone, and 15 to 17 seconds for heave, pitch and roll. Comparable methods for sea wave prediction today reach 10 to 15 seconds. Finally, the signal was filtered in order to obtain better predictions. Although this step seems not to have been performed in previous works, it allowed the Prony method to achieve an average of 20 seconds and 35 seconds for waves and ship motions respectively. Besides, long reliable intervals were obtained, with 95% of successful analyses reaching 30 seconds of prediction for the ship motions. Similar filtering techniques could be implemented for other domains of application.

The Prony analysis was proved to be successful in linear wave theory. The Prony algorithm chosen might play a role in the prediction quality, the matrix-pencil method giving promising results. Besides, the solvers used for linear systems have a great influence on the success of the analysis. Though MATLAB algorithms are efficient, it might be interesting to examine other tools.

Further work should focus on predicting the wave envelope in order to obtain longer predictions. This real-time prediction method then needs to be tested on non-linear waves. Possible recommendations would be to reconstruct the signal with linear terms, but also try a second or a third order wave theory reconstruction. This could later be developed for real wave measurements and vessel motions to assess its efficiency, and the possibility to implement it for actual marine operations.

References

Al-Ani, M., Belmont, M., & Christmas, J. (2019). Statistical Properties of Quiescent Periods from Wave Power Spectral Density. *OCEANS 2019 - Marseille*, 1–5. https://doi.org/10.1109/OCEANSE.2019.8867574

Dalzell, J. F. (1965). A Note on Short-Time Prediction of Ship Motions. *Journal of Ship Research*, *9*(03), 118–121. https://doi.org/10.5957/jsr.1965.9.3.118

Dong, G., Ma, Y., & Ma, X. (2008). Cross-shore variations of wave groupiness by wavelet transform. *Ocean Engineering*, *35*(7), 676–684. https://doi.org/10.1016/j.oceaneng.2007.12.004

Duclos, G., Clément, A., & Chatry, G. (2001). Absorption of Outgoing Waves in a Numerical Wave Tank Using a Self-Adaptive Boundary Condition. *International Journal of Offshore and Polar Engineering*, *11*.

Fernández Rodríguez, A., de Santiago Rodrigo, L., López Guillén, E., Rodríguez Ascariz, J. M., Miguel Jiménez, J. M., & Boquete, L. (2018). Coding Prony's method in MATLAB and applying it to biomedical signal filtering. *BMC Bioinformatics*, *19*(1), 451. https://doi.org/10.1186/s12859-018-2473-y

Giron-Sierra, J. M., & Esteban, S. (2010). The Problem of Quiescent Period Prediction for Ships: A Review. *IFAC Proceedings Volumes*, *43*(20), 307–312. https://doi.org/10.3182/20100915-3-DE-3008.00007

Goda, Y. (1988). Random Seas and Design of Maritime Structures. In *Advanced Series on Ocean Engineering*. World Scientific. https://doi.org/doi:10.1142/7425

Kaplan, P. (1969). A Study of Prediction Techniques for Aircraft Carrier Motions at Sea. *Journal of Hydronautics*, *3*(3), 121–131. https://doi.org/10.2514/3.62814

Nieto Borge, J. C., Rodríguez, G. R., Hessner, K., & González, P. I. (2004). Inversion of Marine Radar Images for Surface Wave Analysis. *Journal of Atmospheric and Oceanic Technology*, *21*(8), 1291–1300. https://journals.ametsoc.org/view/journals/atot/21/8/1520-0426_2004_021_1291_iomrif_2_0_co_2.xml

Prony, R. (1795). Essai expérimental et analytique sur les lois de la dilatabilité des fluides élastiques et sur celles de la force expansive de la vapeur de l'alkool, à différentes températures. *Journal de l'École Polytechnique*, *1*, 24–76.

Sherman, B. W. (2007). *The Examination and Evaluation of Dynamic Ship Quiescence Prediction and Detection Methods for Application in the Ship-Helicopter Dynamic Interface* [Virginia Polytechnic Institute]. http://hdl.handle.net/10919/32436

Yumori, I. (1981). Real Time Prediction of Ship Response to Ocean Waves Using Time Series Analysis. *OCEANS 81*, 1082–1089. https://doi.org/10.1109/OCEANS.1981.1151574

Zygarlicki, J., & Mroczka, J. (2012). Variable-Frequency Prony Method in the Analysis of Electrical Power Quality. *Metrology and Measurement Systems*, *19*. https://doi.org/10.2478/v10178-012-0003-1

Appendices

Appendix 1: Proof that a wave signal is stretched in the time domain and in its amplitude when the peak period and the significant wave height of the JONSWAP spectrum are multiplied by a certain factor

Appendix 2: Mean length and total proportion of QPs that are in common between heave and pitch, displayed in three dimensions

Appendix 3: Mean length and total proportion of QPs that are in common between the three motions - less restrictive threshold for heave (first figure) and three different restrictions (second figure)

Appendix 4: Errors and predicted times on a Prony analysis with a perfect approximation

Appendix 5: Prediction quality as a function of the number of sample points and the approximation end time, in the case $\pi = 0.85$ (first figure); as a function of the number of exponential components and the approximation end time, in the case $n_s = 1000$ (second figure), for **100** components in the original signal

Appendix 6: Influence of high frequency filtering on the prediction quality, in the case $n_s = 1,000$; $t_1 = 300\ s$; $\pi = 0.85$

Appendix 1: Proof that a wave signal is stretched in the time domain and in its amplitude when the peak period and the significant wave height of the JONSWAP spectrum are multiplied by a certain factor

Let us consider here a wave signal $X_1(t)$ created from a JONSWAP spectrum $S_1(\omega)$ with parameters H_s and ω_p. A second signal is created from a spectrum $S_2(\omega)$ with parameters $a \cdot H_s$ and $b \cdot \omega_p$. Both signals are created with the same numbers of components, n. We want to show that this signal is equal to $X_2(t) = aX_1(bt)$: it is stretched both in amplitude and time by the same factors.

The n components are equally distributed between a minimum and a maximum frequency, respectively ω_1 and ω_2. These frequencies are chosen according to ω_p, so that they fit the spectrum window. They are chosen of the form: $\omega_1 = k_1 \omega_p$ and $\omega_2 = k_2 \omega_p$.

The frequency interval between two components is equal to $\Delta\omega = \frac{\omega_2 - \omega_1}{n-1} = \omega_p \frac{k_2 - k_1}{n-1}$, and component number $j \in [\![1; n]\!]$ has a frequency $\omega_j = \omega_1 + (j-1)\Delta\omega = \omega_p \cdot \left(k_1 + (j-1)\frac{k_2 - k_1}{n-1}\right)$, which is directly proportional to ω_p. Thus, the component number j in the second signal has a frequency $\omega_j^2 = b\omega_j^1$, and the frequency interval of the second signal is equal to $\Delta\omega^2 = b\Delta\omega^1$ (the 2 denotes the second signal and not a square).

First, we can calculate the amplitude of the spectrum density of component number j in the second signal with equation (1):

$$S_2(\omega_j^2) = S_2(b\omega_j^1) = \beta(aH_s)^2 \frac{(b\omega_p)^4}{(b\omega_j^1)^5} \exp\left[-\frac{5}{4}\left(\frac{b\omega_j^1}{b\omega_p}\right)^{-4}\right] \cdot \gamma^r$$

$$= \frac{a^2}{b} \beta H_s^2 \frac{\omega_p^4}{(\omega_j^1)^5} \exp\left[-\frac{5}{4}\left(\frac{\omega_j^1}{\omega_p}\right)^{-4}\right] \cdot \gamma^r$$

$$= \frac{a^2}{b} S_1(\omega_j^1).$$

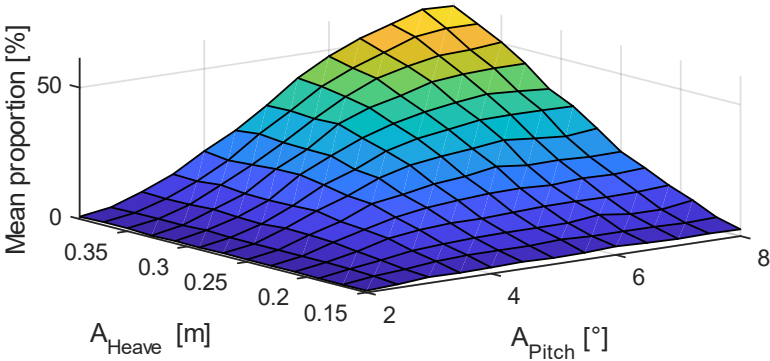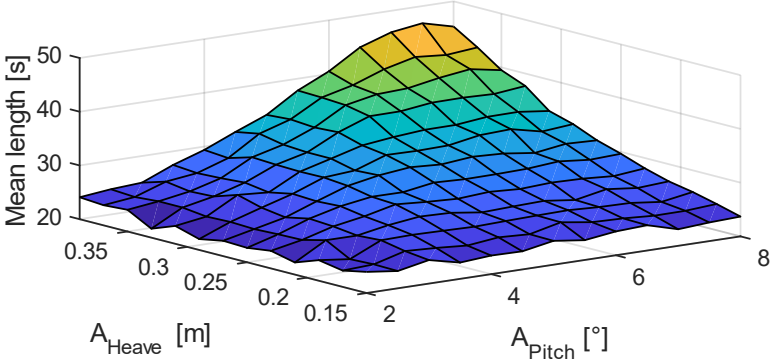Then with (2) we obtain the amplitude A_j^2 of component j in the second signal:

$$A_j^2 = \sqrt{2S_2(\omega_j^2)\Delta\omega^2}$$

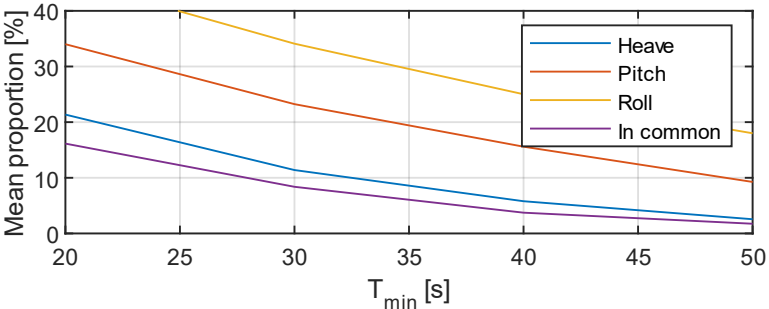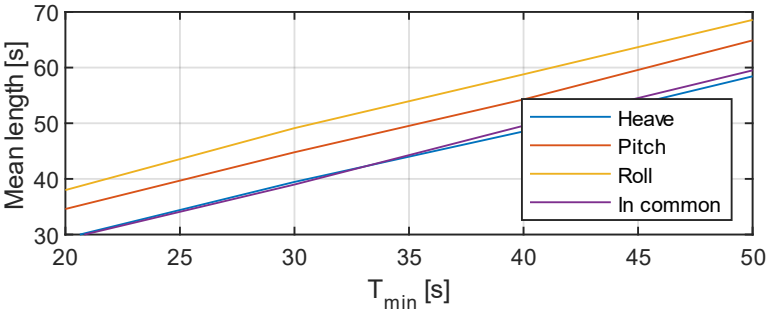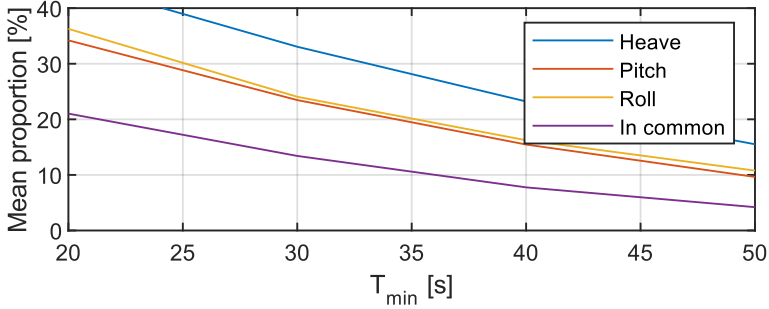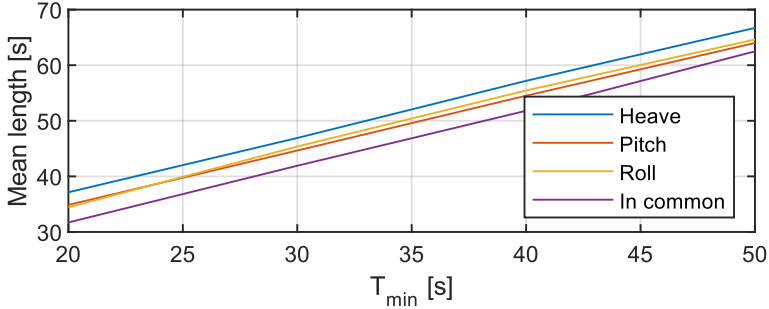$$= \sqrt{\frac{a^2}{b}S_1(\omega_j^1)b\Delta\omega^1}$$

$$= aA_j^1.$$

Finally, the second signal is equal to:

$$X_2(t) = \sum_{j=1}^{n} A_j^2 \cdot \cos(\omega_j^2 t + \varphi_j)$$

$$= \sum_{j=1}^{n} aA_j^1 \cdot \cos(b\omega_j^1 t + \varphi_j) = aX_1(bt).$$
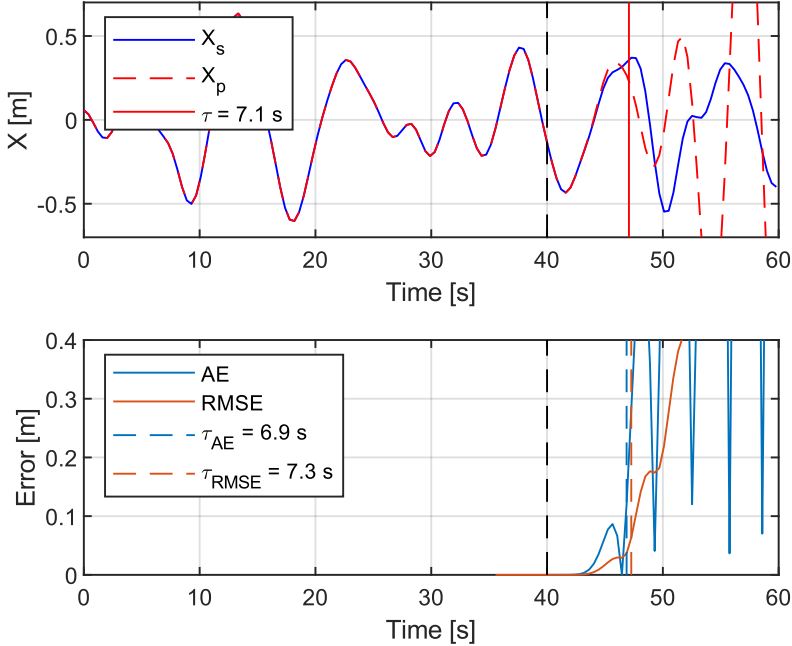
Appendix 2: Mean length and total proportion of QPs that are in common between heave and pitch, displayed in three dimensions
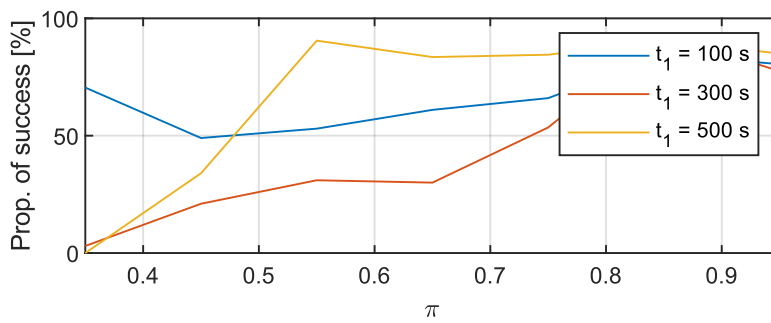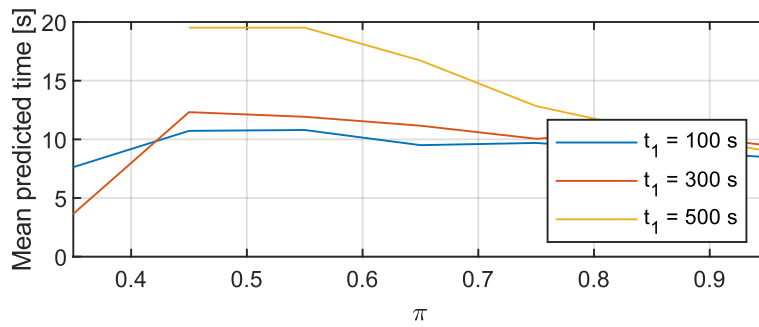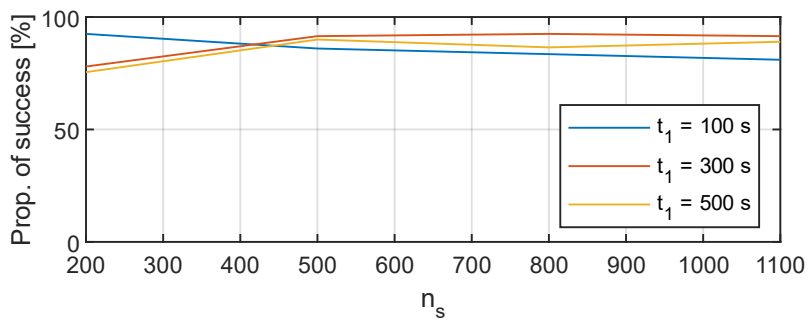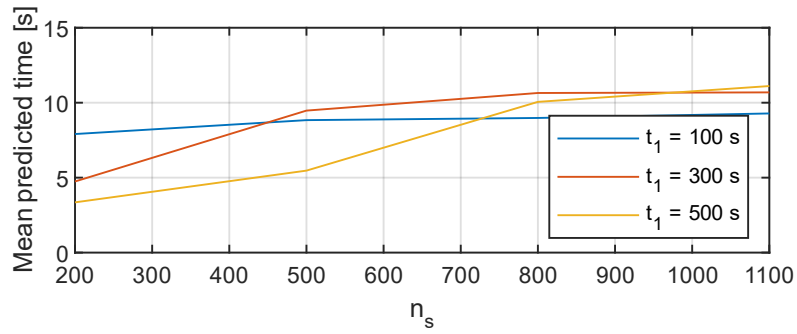
Appendix 3: Mean length and total proportion of QPs that are in common between the three motions - less restrictive threshold for heave (first figure) and three different restrictions (second figure)
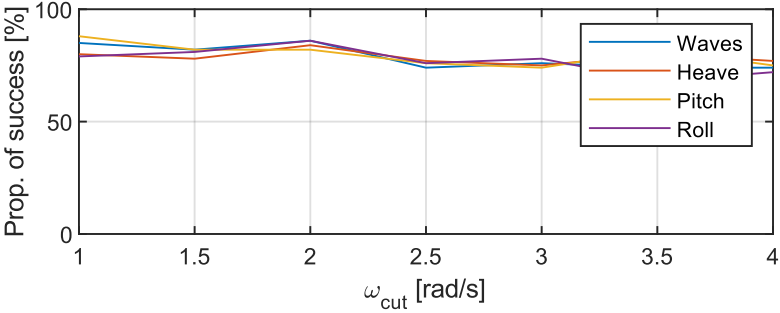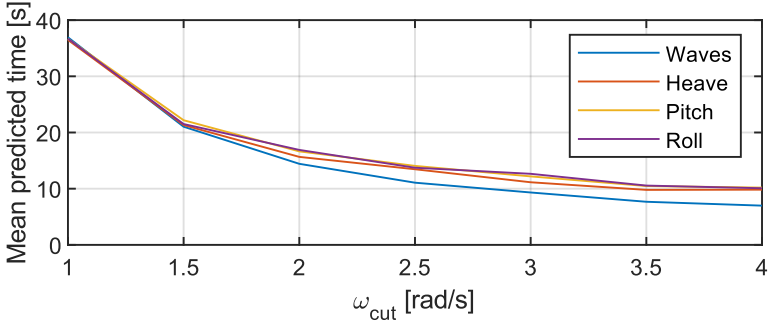
Appendix 4: Errors and predicted times on a Prony analysis with a perfect approximation
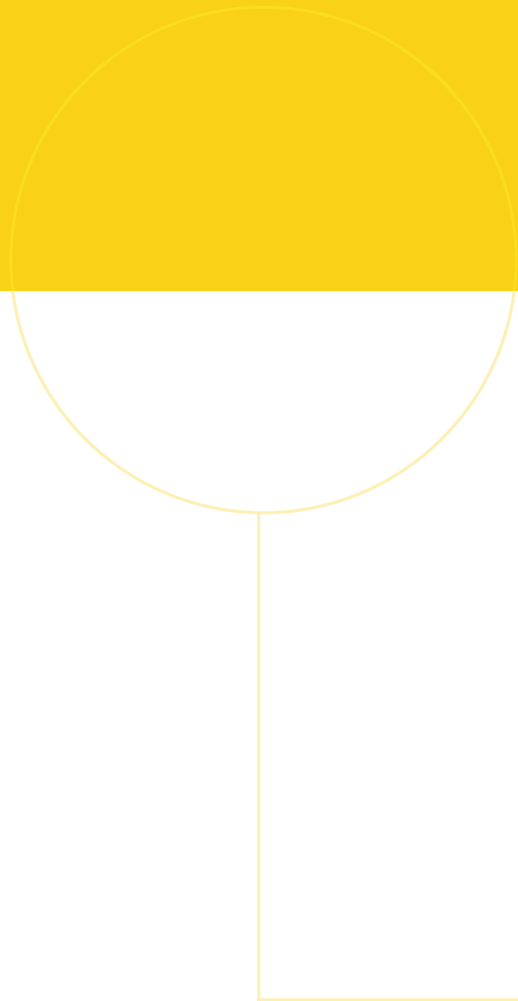
Appendix 5: Prediction quality as a function of the number of sample points and the approximation end time, in the case $\pi = 0.85$ (first figure); as a function of the number of exponential components and the approximation end time, in the case $n_s = 1000$ (second figure), for 100 components in the original signal

Appendix 6: Influence of high frequency filtering on the prediction quality, in the case $n_s = 1,000$; $t_1 = 300\ s$; $\pi = 0.85$